



1 **Fluorescent Biological Aerosol Particle Measurements at a Tropical High Altitude Site in**  
2 **Southern India during Southwest Monsoon Season**

3 A. E. Valsan<sup>1,\*</sup>, R. Ravikrishna<sup>2</sup>, C. V. Biju<sup>3</sup>, C. Pöhlker<sup>4</sup>, V. R. Després<sup>5</sup>, J. A. Huffman<sup>6</sup>, U.  
4 Pöschl<sup>7</sup>, and S. S. Gunthe<sup>1,\*\*</sup>

5

6 <sup>1</sup>EWRE Division, Department of Civil Engineering, Indian Institute of Technology Madras,  
7 Chennai – 600 036, India.

8 <sup>2</sup>Department of Chemical Engineering, Indian Institute of Technology Madras, Chennai – 600  
9 036, India.

10 <sup>3</sup>Department of Civil Engineering, College of Engineering Munnar, PB.No:45, County Hills,  
11 Munnar – 685612, India.

12 <sup>4</sup>Biogeochemistry Department, Max Planck Institute for Chemistry, P. O. Box Number 3060,  
13 Mainz, Germany.

14 <sup>5</sup>Institute of General Botany, Johannes Gutenberg University, Mainz, Germany.

15 <sup>6</sup>Department of Chemistry and Biochemistry, University of Denver, 2190 E. Iliff Ave., Denver,  
16 CO, 80208, USA.

17 <sup>7</sup>Multiphase Chemistry Department, Max Planck Institute for Chemistry, P. O. Box 3060, Mainz,  
18 Germany

19

20

21 To whom correspondence should be addressed:

22 \* Aswathy E. Valsan (aswathyerat@gmail.com)

23 \*\* Sachin S. Gunthe ([s.gunthe@iitm.ac.in](mailto:s.gunthe@iitm.ac.in))

24



## 25 Abstract

26 Primary Biological Aerosol Particles (PBAPs) like fungal spores, bacteria, pollen, etc. are  
27 reported to constitute large fraction of the atmospheric aerosols. They are responsible for the  
28 spread of organisms and diseases throughout the biosphere and may impact atmospheric  
29 processes and the hydrological cycle by acting as ice nuclei (IN) and giant cloud condensation  
30 nuclei (CCN). Despite their importance in the biosphere and climate, continuous measurements  
31 of PBAPs in high time and size resolutions are not available for the Indian subcontinent. Here we  
32 report the first measurements of fluorescent biological aerosol particles (FBAPs) in India. The  
33 measurements were carried out using an ultraviolet aerodynamic particle sizer (UV-APS) in  
34 Munnar, a high altitude tropical site in southern India. The study was conducted for three  
35 consecutive months during the Southwest monsoon season (1.June.2014 – 21.August.2014),  
36 which is marked by heavy and persistent rainfall and strong Westerly/Southwesterly clean winds.

37 Averaged over the entire campaign arithmetic mean number and mass concentrations of coarse-  
38 mode FBAP ( $> 1 \mu\text{m}$ ) were  $0.02 \text{ cm}^{-3}$  and  $0.24 \mu\text{g m}^{-3}$ , respectively, which corresponded to  $\sim 2$   
39 and 6 % of total aerosol loading, respectively. Average FBAP number size distribution exhibited  
40 a peak at  $\sim 3 \mu\text{m}$ , which was most likely contributed by fungal spores, as supported by scanning  
41 electron microscope (SEM) images, and the results are consistent with previous studies made for  
42 FBAP. During eleven weeks of measurements the corresponding total (TAP) coarse mode  
43 particle number concentration was highly variable in contrast to the variability observed in  
44 FBAP number concentration. Averaged over the entire campaign the TAP number and mass  
45 concentrations were  $1.8 \text{ cm}^{-3}$  and  $7.0 \mu\text{g m}^{-3}$ . The TAP and FBAP number concentrations  
46 measured at this site were strongly dependent on changes in wind direction and rainfall. During  
47 the period of continuous and persistent rainfalls the TAP and FBAP concentration exhibited very



48 low concentration levels ( $1.3 \text{ cm}^{-3}$  and  $0.005 \text{ cm}^{-3}$ , respectively) with no observed diurnal  
49 variations. Averaged over the entire campaign FBAP exhibited a moderately diurnal variation  
50 with highest concentration during early morning hours ( $\sim 06:00 - 08:00$  hrs). The campaign  
51 averaged FBAP number concentrations were shown to correlate with daily patterns of  
52 meteorological parameters and were positively correlated with relative humidity (RH;  $R^2=0.58$ ),  
53 and negatively with temperature ( $R^2=0.60$ ) and wind speed ( $R^2=0.60$ ). We did not observe any  
54 significant positive correlation with precipitation as reported by previous researchers from  
55 selected areas. These measurement results confirms the fact that fraction of PBAPs to TAP is  
56 strongly dependent on size and location and thus may constitute significant proportion of total  
57 aerosol particles.



## 58 **1 Introduction**

59 Aerosols are generally defined as a colloidal system of solid or liquid particles suspended in a  
60 gaseous medium (Fuzzi et al., 1997; Pöschl, 2005) and are ubiquitous in the Earth's atmosphere.  
61 The term "Primary Biological Aerosol Particles" (PBAPs; sometimes also referred as bioaerosols  
62 or biological aerosols), describes a subset of aerosol particles, i.e. the solid airborne particles  
63 originating from biological organisms, including viruses, pollen, microorganisms (bacteria,  
64 fungal spores, etc.) and, protozoa or algae, etc., together with fragments of biological materials  
65 such as animal dander, plant debris etc. (Artaxo and Hansson, 1995; Coz et al., 2010; Després et  
66 al., 2007, 2012; Elbert et al., 2007). Bioaerosols can range in size from a few nanometers to few  
67 hundred micrometers in aerodynamic diameter,  $D_a$ , (Coz et al., 2010; Després et al., 2012; Jones  
68 and Harrison, 2004; Matthias-Maser and Jaenicke, 1994) with viruses being the smallest in size  
69 amongst the PBAPs followed by bacterial and fungal spores, while pollen, and plant and animal  
70 fragments represent the largest in size. Depending upon size and ecosystem PBAPs can  
71 constitute 14 – 70% of total number of coarse mode particles and around 20 – 24 % of total mass  
72 of  $PM_{10}$  (particulate matter with size  $\leq 10 \mu m$ ; Elbert et al., 2007; Després et al., 2012; Pöschl et  
73 al., 2010; Huffman et al., 2012). Bioaerosols are present in the ambient atmosphere either as a  
74 single particle, or as agglomerates (Valsan et al., 2015) and exhibit a variety of shapes and  
75 morphological characteristics. Further, it is likely that the surface structure, ice nucleating  
76 proteins, and other characteristics influence substantially the heterogeneous ice nuclei formation  
77 at various temperature levels (Morris et al., 2004, 2014) and they can also act as giant cloud  
78 condensation nuclei (GCCN) thus affecting the hydrological cycle (Andreae and Rosenfeld,  
79 2008; Möhler et al., 2007). Other bioaerosols like pollen or fungal spores are often using air as  
80 the transport medium for distribution and transfer of genetic material and thus can travel and get



81 transported over large distances (Huffman et al., 2010; Elbert et al., 2007; Hallar et al., 2011;  
82 Burrows et al., 2009). A side effect of such a transport and distribution, however, is that they are  
83 produced and spread in large quantities and play an important role in public health as they can  
84 cause allergies. Pathogenic fungi have long been recognized as major threats to animal health  
85 and plants including crops severely jeopardizing the food security (Fisher et al., 2012 and  
86 references therein).

87 Since the last century numerous studies have been conducted in different parts of the world to  
88 understand the abundance and diversity of bioaerosols using various sampling and measurement  
89 techniques, however confining to traditional methods. The last decade has experienced a  
90 substantial development and application of advanced online and offline techniques for studying  
91 characteristic properties of bioaerosols in the field and laboratory (Fröhlich-Nowoisky, et al.,  
92 2009; DeLeon-Rodriguez et al., 2013; Prenni et al., 2009; Huffman et al., 2010, 2012, 2013;  
93 Schumacher et al., 2013; Pöhlker et al., 2012, 2013).

94 Instruments utilizing laser-induced fluorescence (LIF) have been frequently deployed to the  
95 field, enabling real-time characterization of the number size distribution of PBAPs in high time  
96 and size resolution. However, instruments based on LIF do not provide detailed information  
97 about PBAPs, but rather provide broadly categorized information due to a mixture of biological  
98 fluorophores, each detected with varying efficiency (Pohlker et al., 2012, 2013). Most FBAP  
99 measurements have shown that the dominant size range for PBAPs number size distribution is 1  
100 – 4  $\mu\text{m}$  with concentration varying within the factor of 10 (Gabey et al., 2011, 2013; Healy et al.,  
101 2014; Huffman et al., 2010, 2012, 2013; Saari et al., 2015; Schumacher et al., 2013; Toprak and  
102 Schnaiter, 2013; Yu et al., 2016). As studied and described by Huffman et al., (2010) based on  
103 long-term PBAP measurements in central Europe, the signal detected by UV-APS (Ultraviolet



104 Aerodynamic Particle Sizer) in ambient settings was defined as Fluorescent Biological Aerosol  
105 Particles (FBAP), and the resulting quantification of FBAP was further discussed and it was  
106 concluded that FBAP represents an approximate lower limit of actual abundance of PBAPs  
107 present in the ambient air sampled by the UV-APS. Thus, for the consistency and simplicity we  
108 use the similar terminology as suggested by Huffman et al., (2010). Hence the term FBAP is  
109 used as a lower limit proxy for primary biological aerosol particles (PBAPs), biological aerosols,  
110 biological aerosol particles, bioaerosols and similar terms mentioned in this study.

111 Despite such instrumental advancements described above, the studies related to the  
112 quantification of bioaerosols and their role in climate and human health have been extremely  
113 limited in space and time. Particularly, for the Indian subcontinent, which constitute around  
114 ~18% of the world's total population, studies related to the bioaerosols are relatively few with  
115 spotty analysis performed only by traditional techniques (Bhati and Gaur, 1979; Chakraborty et  
116 al., 1998; Gangamma, 2014; Srivastava et al., 2012; Sharma and Rai, 2008; Pachauri et al., 2013;  
117 Valsan et al., 2015; Ansari et al., 2015; Adhikari et al., 2004). Thus, sources, abundance, and  
118 properties of bioaerosols, which are strongly dependent on location and season, remains poorly  
119 characterized over the Indian subcontinent and need to be addressed systematically.

120 Investigating and quantifying the role of bioaerosols over the Indian continent is not only  
121 important because of the scarcity in the literature but also due to its unique climatic condition  
122 experienced by the two Monsoon seasons associated with two distinct synoptic scale wind  
123 patterns. Indian agriculture is strongly dependent on the Southwest Monsoon, and is the largest  
124 livelihood provider in India and contributes a significant figure to the Gross Domestic Product  
125 (GDP). Therefore, it is very important to better understand and quantify the role of bioaerosols in  
126 cloud and precipitation formation during Monsoon and convective rainfall. The concentrations of



127 fluorescent aerosol was shown to increase during and after rainfall in a semi-arid forest in the  
128 Western US (Huffman et al., 2013), but the same pattern was not observed in a similar study in  
129 the Amazon basin (Huffman et al, 2012). Thus, the bioaerosols emitted during monsoon season  
130 could potentially play an important role in cloud and precipitation formation as shown by Ansari  
131 et al. (2015). Additionally, bioaerosols over the Indian sub-continent can have a direct societal  
132 impact where huge set of population may directly get affected by the spread of diseases and  
133 covertly due to the loss in agricultural output.

134 Thus, studies involving characterization of bioaerosols using advanced techniques over this  
135 region are important to understand and quantify the impact of bioaerosols on regional  
136 biodiversity with larger implication towards human and ecosystem health. With this motivation  
137 we have deployed an UV-APS for the detection and measurement of number size distribution of  
138 PBAPs at a high-altitude site of Munnar in Western Ghats of southern tropical India during  
139 Southwest monsoon season for ~3 months. To our knowledge this study presents the first multi-  
140 month ambient measurement investigations involving UV-APS over the Indian subcontinent.

## 141 **2 Methods**

### 142 **2.1 Site Description**

143 Measurements were performed to sample the air masses (see section 2.2) from a **high-altitude**  
144 **site (Munnar; 10.09°N, 77.06°E; 1605 m amsl – above mean sea level – Fig. 1)** located in the  
145 Western Ghats just 90 km ~~away as the crow flies~~ from Arabian Sea in the Southern part of  
146 tropical India. The observational site is located on a hill with a valley towards the South and a  
147 small mountain towards the North surrounded by dense vegetation including tea gardens and  
148 Eucalyptus trees. Climatologically this region is classified as subtropical highland with dry  
149 winters and is listed as the Shola forest-grass ecosystem as defined in the land-use type



terminology. The Western Ghats, one of the eight mountain ranges in India and identified as ~~one~~  
~~of the hottest hot spots~~ of biodiversity (Myers et al., 2000) in the world, originates near the  
border of Maharashtra and Gujarat running ~1600 km towards South, parallel to the Western  
coast through the states of Gujarat, Maharashtra, Karnataka, Kerala, and Tamilnadu ending at the  
Southern tip of India near Kanyakumari. This mountain range separates the coastal plain from  
the Deccan plateau making Western coastal plain a narrow land strip with a maximum width of ~  
110 – 120 km, sandwiched between the Western Ghats and the Arabian Sea. During the SW  
Monsoon season (June – September) the Southwesterly moisture laden winds are intercepted by  
the Western Ghats causing persistent and heavy rainfall on the windward side of these  
mountains. This causes the wash out and wet deposition of the pollutants in the coastal strip  
(Kerala) emitted due to anthropogenic activities thus bringing clean marine influx with minimum  
impact of anthropogenic emissions (Satheesh and Srinivasan, 2002). Therefore, during this  
particular season this observational site can be regarded as relatively pristine as compared to any  
other operational ~~high-altitude~~ observatory/site in Indian tropical region (Shika et al., 2016).

## 2.2 General Meteorology

Southern India nominally experiences two Monsoon seasons, the Southwest monsoon (SW; June  
– September) and the Northeast monsoon (NE; November – January), which are strongly  
associated with the movement of Inter-Tropical Convergence Zone, the ITCZ (Kanawade et al.,  
2014). The SW monsoon winds are dominant during **June to September** bringing almost  
anthropogenically “clean” (not affected by human activities) marine influx over the continent  
from Arabian Sea when ITCZ moves Northwards reaching 30°N during July (Naja and Lal,  
2002). These air masses originate over the Indian Ocean and travel thousands of kilometers over  
oceanic water, including Arabian Sea, before reaching the observational site. The Southward





173 movement of ITCZ reaching up to equator is associated with NE monsoon, which is also marked  
174 as winter season in India occurring during October to January, when prevailing winds are  
175 predominantly blowing in NE direction. The measurement site of Munnar receives more than  
176 85% of its annual rainfall during SW monsoon season and experiences scattered rainfall events  
177 during NE monsoon season. The detailed meteorological parameters measured during the field  
178 measurement campaign carried out during SW Monsoon season at Munnar are discussed below.

## 179 **2.2 Real-time fluorescence measurement**

180 The biological aerosol particles ~~from a high-altitude relatively pristine site~~ were measured using  
181 an UV-APS (TSI Inc. Model 3314; Serial Number: 71331023) as per the standard instructions  
182 given in the technical manual. The detailed description about the instrument including operating  
183 principles, field operation, data analysis protocol, and critical operational parameters are  
184 discussed elsewhere (Kanaani, et al., 2007, 2008; Agranovski et al., 2003, 2004, 2005; Brosseau  
185 et al., 2000; Huffman et al., 2010, 2012; Hairston et al., 1997).

186 Briefly, the instrument is capable of measuring the aerosol particles in aerodynamic diameter  
187 ( $D_a$ ) range of 0.54 – 19.81  $\mu\text{m}$  over 52 channels by means of measuring the time-of-flight  
188 between two He-Ne red lasers ( $\lambda=633\text{ nm}$ ). Once the particle size is determined, the same  
189 particle is further excited using a third ultraviolet Nd:YAG laser ( $\lambda=355\text{ nm}$ ) and emissions are  
190 measured in the range of 420 – 575 nm. The spectrally unresolved total fluorescence is recorded  
191 for each individual particle in to one of the 64 channels with increasing order of fluorescence  
192 intensity. Huffman et al., (2010) described that the counting efficiency of the instrument drops  
193 below 100% at  $D_a < 0.7\text{ }\mu\text{m}$  (counting efficiency ~50% at 0.54  $\mu\text{m}$ ), hence, the particle number  
194 concentration values reported for particle sizes of  $<0.7\text{ }\mu\text{m}$  are lower limit of the actual  
195 concentration of the air sample. During analysis presented in this paper the particles detected in



the size range of 15 – 20  $\mu\text{m}$  were included and the reported number concentration values should be considered as the lower limit of the actual values present in the air sample, due to limitations in the size calibration for particles of this size. The UV-APS measurement cycle was initiated with 5 minutes interval (including the full diameter range scan for 285 seconds and 15 seconds of back-scanning recording) total of 22280 sampling points during entire measurement campaign) where air sample was drawn with a volumetric flow rate of 5 L  $\text{min}^{-1}$  (lpm) at ambient temperature and pressure. All the times reported in this study are local time pertaining to Indian Standard Time (IST; GMT+5:30).

The UV-APS was placed next to the window inside a room in the College of Engineering, Munnar, Kerala located on a hill. A stain-less steel tubing with  $\frac{3}{4}$ " OD (outer diameter) and TSP inlet was used to construct the inlet unit for air sampling, which was ~9 m and ~2 m above the ground and rooftop, respectively. Thus the sampled air masses were expected to have minimal influence caused by the dynamics associated with the building structure. To minimize the particle losses due to impaction resulting from sharp bends, the electrically conductive silicon rubber tubing (~1.5 m; 12 mm inner diameter) was attached to the stain-less steel tube just outside the window (Fig. S1) avoiding the sharp bends. Before the sampled air was passed to the instrument, diffusion dryer (~1 m) with silica gel (orange color indicating) was used to dry and maintain the relative humidity <40%. Thus combining all the tubing involved in the air sampling the sample flow residence time was calculated to be ~ 20 seconds. The sample flow through all the tubing was expected to be laminar during entire sampling period and hence diffusion losses are expected to be negligible for all the size-ranges of the sampled particles.

For the present study we derived number size distribution of fluorescence biological aerosol particles,  $dN_F/d\log D_a$ , for each size bin by summing up the particle number concentration from



the fluorescence channel numbers 3 – 64 and similarly the total particle number size distribution,  $dN_T/d\log D_a$ , was derived from channel numbers 1 – 64. In the present study we have used 1.0  $\mu\text{m}$  as a cut-off diameter for given  $dN_F/d\log D_a$  and  $dN_T/d\log D_a$  to calculate the fluorescence biological aerosol number and total aerosol number concentrations,  $N_F$  and  $N_T$ , respectively. This is mainly due to the fact that particle counting efficiency of the UV-APS drops below unity at 0.7  $\mu\text{m}$  and the interferences due to fluorescence from non-biological aerosol particles below 1.0  $\mu\text{m}$  can at times be very high (Huffman et al., 2010). Also note that the cutoff at 1  $\mu\text{m}$  moreover represents the border between fine ( $<1\mu\text{m}$ ) and coarse ( $>1\mu\text{m}$ ) modes of the particle number size distribution. The subscripts throughout this manuscript text “F” and “T” refer to fluorescent and total coarse mode particles, respectively. Please refer to Table 1 for the abbreviations, notations, and symbols used in this manuscript. The particle mass size distributions ( $dM/d\log D_a$ ) for total as well as fluorescent biological aerosol particles were calculated for each size bin by multiplying  $dN/d\log D_a$  with volume of an aerodynamically equivalent sphere with the geometric midpoint diameter ( $D_{a,g}$ ) and assuming the unit density ( $1\text{ g cm}^{-3}$ ) and unit shape factor. The integral mass concentrations of coarse fluorescent biological aerosol particles and total coarse particles,  $M_F$  and  $M_T$ , respectively were calculated by integrating the particle mass distribution for  $D_a > 1\mu\text{m}$ ; but should be viewed as first approximation as a result of uncertainty associated with the density and shape of the particles (Huffman et al., 2010).

#### *Fluorescence of submicron particles*

It has been reported by previous researchers that UV-APS is known to exhibit fluorescence for some fraction of non-biological aerosol particles including soot, PAHs, and cigarettes smoke, which could be erroneously counted as FBAP (Huffman et al., 2010; Pan et al., 1999a, 1999b). It has also been emphasized that such interference can mostly occur for particles less than 1  $\mu\text{m}$  as



the contribution from combustion sources at this size range is expected to be dominant. To investigate the contribution of non-biological aerosol particles that are counted as fluorescence biological aerosol particles, Huffman et al., (2010) performed the correlation between the integrated number concentrations of fluorescent particles ( $N_F$ ) and total particles ( $N_T$ ) for different diameter ranges (only for the fluorescence channels  $>3$ ). They found that the correlation for the submicron particles was systematically linear, whereas the correlation for supermicron particles was more random, indicating that a large fraction of submicron particles showing fluorescence might have been originated from anthropogenic sources, which may not be the case for the supermicron particles. To investigate the influence of anthropogenic emissions on submicron particles we performed the similar correlation analysis for the entire campaign and, however, found the different results. The correlation between integrated number concentrations of fluorescent particles ( $N_F$ ) and total particles ( $N_T$ ) for supermicron ( $D_a > 1$ ) and submicron ( $D_a < 1$   $\mu\text{m}$ ) diameter range exhibited a very poor scatter ( $R^2=0.03$  and  $R^2=0.002$  respectively;  $N=22280$ ; Figs. S2) indicating extremely small percentage of fluorescence was contributed by non-biological aerosol particles in supermicron and submicron particle ranges.

Since certain component of the mineral dust may exhibit a weak fluorescence (Huffman et al., 2010; Sivaprakasam et al., 2004; Toprak and Schnaiter, 2013), we performed the separate correlation analysis for a focus period, which was dominated by the transport of mineral dust from West Asia, North Africa, and Arabian region (discussed below). The correlation between integrated number concentrations of  $N_F$  and  $N_T$  for  $D_a > 1$   $\mu\text{m}$  was moderately linear ( $R^2=0.26$ ;  $N=3138$ ; Fig. S3a) compared to submicron size range during the dusty period ( $R^2=0.007$ ;  $N=3138$ ; Fig. S3b). As a result, correlation between  $N_F$  and  $N_T$  indicates that fraction of



264 supermicron particles exhibiting fluorescence may have been contributed by mineral dust, but  
265 this being not the case for submicron particles.

266 From these analyses we infer that the contribution of non-biological aerosol particles exhibiting  
267 fluorescence was negligible in both submicron and supermicron (except during “dusty period”;  
268 discussed below) size ranges. Thus we hypothesize that due to persistent rainfall the submicron  
269 and supermicron particles resulted from combustion and other similar activities, were either  
270 efficiently removed or were not transported to the observational site, indicating that substantial  
271 fraction of the particles in both the size ranges were of biological origin. Thus this observational  
272 site could be potentially termed as relatively pristine and free from anthropogenic emissions  
273 during the monsoon season.

274 Please note, however, that to have the consistency and uniformity in the comparison of  $N_F$ ,  $N_T$ ,  
275 and other similar parameters reported by the previous studies we derived all the statistics  
276 associated with  $dN_F/d\log D_a$  and  $dN_T/d\log D_a$  with a cutoff diameter of 1  $\mu\text{m}$ .

277

### 278 2.3 Meteorological parameter measurement

279 The meteorological parameters in parallel with the UV-APS measurements were recorded during  
280 the entire campaign using an ultrasonic weather sensor (Lufft WS600-UMB) installed on a  
281 rooftop at the same height and a few meters away from the UV-APS inlet (Fig. S1). The weather  
282 station was capable of recording temperature, dew point temperature, relative humidity,  
283 precipitation intensity, wind speed, wind direction, and air pressure and was set to record these  
284 meteorological parameters with every 5 minutes interval with time synchronized to UV-APS  
285 measurement clock. The data from the weather sensor was stored by using an in-house  
286 developed external data logger. The obtained meteorological data was compared with another



287 ultrasonic weather station installed within the close vicinity (Valsala make). The scatter plots  
288 between the data (10 min averaged) obtained from our weather station and the one installed in  
289 the close vicinity exhibited very strong agreement for all the meteorological parameters  
290 measured/recorded (average  $R^2 \geq 0.95$ ).

## 291 **2.4 SEM Analysis**

292 The samples for Scanning Electron Microscopy (SEM) analysis were collected on a 25 mm  
293 Nucleopore® Polycarbonate filter paper with pore sizes of 5  $\mu\text{m}$  and 0.2  $\mu\text{m}$  using a two stage  
294 filtering method as described by Valsan et al., (2015). All samples were collected for  
295 approximately a duration of 60 min at an average flow rate of 5 lpm and were stored in air-tight  
296 container at 4°C until SEM analysis. The five samples collected during the entire campaign were  
297 analyzed using two different scanning electron microscopes. 1. Quanta FEG 200 located at the  
298 Sophisticated Analytical Instrument Facility (SAIF) and 2. Hitachi S 4A00 located at the  
299 Chemical Engineering Department of Indian Institute of Technology Madras. Before loading the  
300 filter paper on to the studs, they were cut into small squares of  $\sim 1\text{ cm}^2$  and sputter coated with  
301 gold particles. The biological aerosol particles were identified purely based on their  
302 morphological features adopting the method suggested by Matthias-Maser and Jaenicke  
303 (1991,1994). Detailed description on sample collection and analysis was discussed elsewhere  
304 (Valsan et al., 2015).

## 305 **3 Results and discussions**

### 306 **3.1 Campaign overview**

307 Figure 2 shows the temporal evolution and variability of the several parameters characteristic for  
308 the meteorological conditions, FBAP, and TAP properties observed throughout the measurement  
309 campaign during SW monsoon season at a high-altitude site of Munnar.



Overall the meteorological conditions during the campaign at Munnar can be summarized as follows: The predominant wind direction was observed to be Westerly/Southwesterly (Fig. 1), which characterizes the monsoon season bringing almost anthropogenically clean marine influx (Vinoj and Satheesh, 2003) over the continent marked by presence of persistent rainfall, high relative humidity (RH), higher wind speeds, and lower temperatures. During this period the diurnal variations in temperature and relative humidity were totally absent and temperatures almost approached the dew point temperature. Further, the Westerly/Southwesterly air masses arriving at the observational site were free from any anthropogenic influence and were laden with dust and sea salt particles (Satheesh and Srinivasan, 2002; Vinoj et al., 2014; Prospero, 1979). On few occasions, however, Northerly winds were also observed, which was associated with calm winds, lower RH levels, higher temperatures, and reduced rainfall. During Northerly winds the temperature exhibited relatively more pronounced diurnal variations compared to the relative humidity. The average meteorological parameters (arithmetic mean $\pm$ standard deviation) recorded during entire measurement period were: (840 $\pm$ 1.3) hPa absolute pressure, (17.2 $\pm$ 1.4) $^{\circ}$ C ambient temperature, (96.4 $\pm$ 5.7) % relative humidity, (2.8 $\pm$ 1.3) m s $^{-1}$  local wind speed, (270) $^{\circ}$  local wind direction (vector mean weighted by wind speed), and (4188) mm of accumulated rainfall.

The total of more than five months of bioaerosol measurements in high time and size resolution were performed at this site comprising two contrasting seasons, monsoon (dominated by Southwesterly winds) and winter (dominated by Northeasterly winds). In this study we present the results from the field campaign carried out during the SW monsoon season whereas the detailed results from the winter campaign from the same measurement site will be presented in the follow up study. We first discuss the characteristic features of the time series as a broad



overview of the observed concentration levels, variability, and trends in  $N_T$  and  $N_F$ . Figure 2 (f,g,h,i,j) shows time series of geometric mean diameter ( $D_g$ ),  $N_F$ ,  $N_F/N_T$ ,  $N_T$ , FBAP and TAP 3-D and the size distribution measured with the UV-APS for the entire campaign. Throughout the measurement period the hourly averaged  $D_g$  time series consistently remained in the range of  $\sim 2 - 4 \mu\text{m}$  with almost no diurnal variations. During the second half of the campaign, the  $D_g$ , however, exhibited relatively high variability with average mean diameter of  $2.6 \pm 0.7 \mu\text{m}$ . Unlike the  $N_T$  and  $N_F$  the variability in  $D_g$  was observed to be not affected by meteorological parameters except for wind direction (see section 3.6.1) on few occasions. The total coarse particle number concentration,  $N_T$ , exhibited high and consistent variability during entire measurement period, however, with no distinct diurnal cycle. Averaged (arithmetic mean  $\pm$  standard deviation) over the entire measurement period  $N_T$  was observed to be  $1.8 \pm 1.5 \text{ cm}^{-3}$  with lowest and highest concentrations of  $0.01 \text{ cm}^{-3}$  and  $8.6 \text{ cm}^{-3}$ , respectively. The average  $N_T$  concentration during the months of June, July, and August was  $2.7 \pm 1.9 \text{ cm}^{-3}$ ,  $1.5 \pm 0.96 \text{ cm}^{-3}$ , and  $0.96 \pm 0.77 \text{ cm}^{-3}$ , respectively, with highest and lowest values for individual months respectively as follows: June:  $8.6$  and  $0.04 \text{ cm}^{-3}$ , July:  $5.1$  and  $0.02 \text{ cm}^{-3}$ , and August:  $3.6$  and  $0.01 \text{ cm}^{-3}$  (Fig. S4). The monthly averaged  $N_T$  concentration exhibited the decreasing trend from June to August as the monsoon progressed (Tab. 2). In contrast to the total aerosol particle number concentration,  $N_F$ , exhibited less pronounced but episodic peaks in the time series during majority of the measurement period resulting in modest variability and campaign arithmetic mean value was  $0.02 \pm 0.02 \text{ cm}^{-3}$ . The highest  $N_F$  concentration of  $\sim 0.52 \text{ cm}^{-3}$  was observed on 3<sup>rd</sup> of June (and few more occasions) whereas the lowest  $N_F$  concentration was consistently observed on more than one occasion during the months of July and August. The average  $N_F$





concentration during June and August was  $0.03 \pm 0.03 \text{ cm}^{-3}$  and  $0.015 \pm 0.02 \text{ cm}^{-3}$ , respectively with lowest  $N_F$  concentration of  $0.007 \pm 0.006 \text{ cm}^{-3}$  in July (Tab. 2).

The time series of relative contribution of FBAP to TAP number,  $N_F/N_T$ , most of the time during campaign exhibited the similar temporal variability to  $N_F$ . The pronounced extreme values of  $N_F/N_T$  observed on few occasions resulted from strong variability in the concentrations of  $N_T$  rather than resulting from the variations in the concentrations of  $N_F$ , indicating the inverse correlation between  $N_T$  and  $N_F/N_T$ . Huffman et al., (2010) have also reported the similar inverse correlation between  $N_T$  and  $N_F/N_T$  from the measurements carried out at a semi-urban site from central Europe. Temporal evolution of  $N_F$ ,  $N_F/N_T$ , and 3-D number size distribution for individual campaign months is shown in Fig. S5. A campaign overview of FBAP mass concentrations and 3-D size distribution for each five minutes of UV-APS sample averaged over the entire measurement period and individual months are shown in Figure S6. During the first month of measurement campaign  $M_F$  exhibited high concentration with sporadic spikes at irregular intervals with broader size distribution ( $\sim 2 - 8 \mu\text{m}$ ) towards the end of the month (with highest concentration  $\sim 6.0 \mu\text{g m}^{-3}$ ). As the measurement campaign progressed, with arrival of persistent and heavy rainfall (whole of July and first-half of August)  $M_F$  exhibited a gradual decrease with minimum value reaching as low as  $6 \times 10^{-4} \mu\text{g m}^{-3}$ . After a period of consistent low mass concentration, during the last week of measurement campaign,  $M_F$  exhibited an increase with highest mass concentration of  $\sim 5.8 \mu\text{g m}^{-3}$ , which coincided with reduced and scattered rainfall.

### 3.2 Particle number and mass concentrations

#### 3.2.1 Statistical distribution of number concentrations

Statistical distribution of five-minute number concentration measurements carried out at Munnar over the course of the campaign are shown in Fig. 3 and tabulated in Tab. 2. Over the entire



measurement period the monthly mean of  $N_T$  varied by a factor  $\sim 3$  from minimum in August (0.96 cm<sup>-3</sup>) to a maximum in June (2.7 cm<sup>-3</sup>). In addition to the highest concentration, the variability of  $N_T$  was also found to be highest in the month of June as can be seen from the size of the 5 – 95<sup>th</sup> percentile bars in Fig. 3a. The relative high variability in  $N_T$  for entire measurement period was largely contributed by the variability in  $N_T$  observed in the month of June. During the initial phase of Southwest monsoon season the predominant Westerly/Southwesterly winds are known to transport the mineral dust, which constitute large fraction of coarse mode (also in larger diameter size of fine mode fraction) TAP concentration, over the continental region (Vinoj et al., 2010, 2014; Li and Ramanathan, 2002; Satheesh and Srinivasan, 2002; Vinoj and Satheesh, 2003). As the monsoon progresses the persistent rainfall can cause the washout of these dust particles along the path of monsoonal rain, thus reducing the coarse mode TAP concentration (Pranesha and Kamra, 1997a,b; Radke et al., 1980; Moorthy et al., 1991). The monthly arithmetic mean and median average of  $N_T$  did not exhibit significant differences. The monthly mean values of  $N_F$  varied by the factor of  $\sim 4$  with consistently high variability during all the observational months. Similar to  $N_T$ , the monthly mean average value and variability in  $N_F$  was highest in the month of June, with mean of  $0.03 \pm 0.03$  cm<sup>-3</sup> and high size of 95<sup>th</sup> percentile (with value of 0.086 cm<sup>-3</sup>), respectively. The lowest average concentration in  $N_F$  ( $0.007 \pm 0.006$  cm<sup>-3</sup>) observed in the month of July was associated with relatively lower variability as compared to other months of field measurement campaign. Unlike  $N_T$ , the arithmetic mean and median average of  $N_F$  for individual months exhibited a significant difference as can be seen from the box plot shown in Fig. 3b. The variability of  $N_F/N_T$  showed the similar temporal pattern as that of  $N_F$ , except that campaign average mean  $N_F$  concentration was higher than that of the August, whereas the campaign averaged mean  $N_F/N_T$  was observed to



401 be lower than the mean calculated for August. As can be seen from Fig. 3c, the mean relative  
402 contribution of  $N_F$  to  $N_T$  was lowest in the month of July ( $\sim 1\%$ ) and highest in the month of June  
403 and August ( $\sim 3\%$ ). The median and mean for  $N_F/N_T$ , over the course of campaign were  $\sim 1$  and  
404  $2\%$ , respectively. The average values of  $N_F/N_T$  over this part of the globe were found to be lower  
405 as compared to previously investigated sites (Huffman et al., 2010, 2012; Bowers et al., 2009;  
406 Schumacher et al., 2013; Matthias-Maser and Jaenicke, 1995; Matthias-Maser et al., 2000;  
407 Gabey et al., 2010).

#### 408 *Diurnal patterns of the number concentration*

409 The average diurnal trends for three individual months and the entire measurement campaign  
410 were analyzed. Figure 4 shows the median FBAP values for each hour of the day for three  
411 individual months and entire campaign, and Fig. S7 shows the corresponding TAP plots. Overall  
412  $N_F$  exhibited a moderately diurnal pattern with consistent early morning (06:00 hr) peak at  $\sim 3$   
413  $\mu\text{m}$  (Fig. 4a) where in the month of July this early morning peak was absent. A relatively weak  
414 peak during late evening (20:00 hr) in FBAP concentration at  $\sim 3 \mu\text{m}$  was consistently observed  
415 in the month of July. In the month of June the average diurnal  $N_F$  concentration started increasing  
416 early in the evening ( $\sim 18:00$  hr), which gradually increased through the night and reaching  
417 maximum at  $\sim 06:00$  hr and started decreasing thereafter as day progressed. The average diurnal  
418  $N_F$  pattern in August exhibited more or less qualitatively similar features to that of diurnal pattern  
419 observed in June. In general the weak diurnal pattern observed in  $N_F$  during the month of July  
420 was consistent with weak RH and temperature diurnal patterns, and persistent rainfall observed  
421 during July. The early morning peak at  $\sim 3 \mu\text{m}$  on the diurnal scale was also reported from  
422 pristine Amazonian rainforest environment (Huffman et al., 2012). Corresponding average size  
423 distributions for entire measurement period will be discussed in details in Sec. 3.3. The diurnal



variations of  $N_T$  (Fig. S7), on the other hand were very distinct from those of  $N_F$ . The size resolved  $dN_T/d\log D_a$  for each individual months exhibited a consistent and flat concentration profile at  $<1 \mu\text{m}$ , except for the month of August where a pronounced afternoon peak ( $\sim 12:00$ ) at  $\sim 1 \mu\text{m}$  was observed. Reduced rainfall and substantial changes in meteorological parameters including the change in prevailing wind speed and shift in direction during later half of August might have caused the appearance of afternoon peak due to particles resulting from local sources. As like  $N_F$ ,  $N_T$  showed the strong quantitative variability amongst each individual month (Fig. S7). Previous studies where similar instrument was used have reported that pronounced diurnal variations in  $N_T$  are strongly coupled with diurnal variations in meteorological variables especially mixing layer depth (Garland et al., 2009; Raatikainen et al., 2014; Du et al., 2013). The absence of pronounced diurnal variations in  $N_T$  at this particular site may be a result of weak dependence of coarse mode TAP concentrations on meteorological parameters combined with persistent rainfall causing the washout of these particles (Radke et al., 1980; Raatikainen et al., 2014; Kanawade et al., 2014; Shika et al., 2016). This also indicates the absence of any strong and localized source of anthropogenic emissions during most of the campaign period. Diurnal patterns of  $N_F/N_T$  more or less followed the same pattern as that of  $N_F$  during all the measurement months owing to complete absence of diurnal variability in  $N_T$ . Averaged over the entire campaign the  $N_F/N_T$  was found to be highest during early morning hour at  $\sim 06:00$  hr ( $\sim 3.2\%$ ) consistent with the time of high  $N_F$  concentration (Fig. 4). The distinct diurnal pattern in  $N_F$  and  $N_T$  supports the fact that the sources of TAP and FBAP were different over this region.

### 3.2.2 Statistical distribution of mass concentration

Basically UV-APS measures the particle number; the average mass of size-resolved particles can be derived as first approximation by assuming the particle density equal to  $1 \text{ g cm}^{-3}$  (unit



density). Accordingly the overview of mass concentration of FBAP over the course of measurement period is presented here. The statistical distribution of five minutes mass concentration derived from number concentration measurements over the course of campaign is shown in Fig. 5 and tabulated in Tab. 2. The monthly mean values of  $M_T$  exhibited the similar trend and temporal variability as that of  $N_T$  with overall decrease in  $M_T$  through the course of measurement months as campaign progressed. The highest monthly average concentration of  $M_T$  ( $\sim 10.6 \mu\text{g m}^{-3}$ ) was observed in the month of June whereas the lowest  $M_T$  of  $\sim 4.2 \mu\text{g m}^{-3}$  was observed in the month of August. Averaged over the entire measurement period the mean  $M_T$  at Munnar was  $\sim 7 \mu\text{g m}^{-3}$ , which was comparable to the values reported from central European city ( $M_T \sim 7.3 \mu\text{g m}^{-3}$ ) and higher than concentration of  $M_T$  ( $\sim 2.5 \mu\text{g m}^{-3}$ ) reported from pristine Amazonian rainforest region measured during wet season (Huffman et al., 2010; 2012). The monthly mean values of  $M_F$ , on the other hand, did not exhibit similar pattern like  $M_T$ , but followed temporal pattern like  $N_F$ . The highest mean mass concentration of  $M_F$  ( $\sim 0.4 \mu\text{g m}^{-3}$ ) observed during June and was  $\sim 3$  and  $2$  times lower than the concentrations observed at a central European city ( $\sim 1.26 \mu\text{g m}^{-3}$ ) and pristine Amazonian rainforest ( $\sim 0.85 \mu\text{g m}^{-3}$ ), respectively. The higher difference between mean and median values of the box plots indicates the higher temporal variability. The relative difference between mean and median of  $N_F$  was found be higher than that of  $M_F$  indicating higher temporal variability of  $N_F$  during all measurement months. Averaged over the course of entire measurement period this trend was found to be consistent. The median and mean for  $M_F/M_T$  over the course of entire measurement period were  $6$  and  $3\%$  respectively, which is relatively low compared to previously reported studies for various other environments (Huffman et al., 2010; 2012; Artaxo and Hansson, 1995; Schumacher et al., 2013). On average the relative contribution of FBAP to TAP coarse mode



470 particle mass was ~3 times higher (~6%) than its contribution to coarse mode particle number  
 471 concentration (~2%). This is consistent with the observations that FBAPs show enhanced  
 472 prevalence among the larger aerosol particles (Huffman et al., 2010).

473 *Diurnal patterns of mass concentration*

474 The diurnal trends in  $M_F$  for individual months and campaign average were also analyzed and are  
 475 shown in Fig. 6. The corresponding diurnal trends in  $M_T$  are shown in Fig. S8. The monthly  
 476 averaged diurnal trends in  $M_F$  for individual months and entire campaign exhibited similar trend  
 477 corresponding to  $N_F$ . However, the prominent peak in  $dM_F/d\log D_a$  was observed at higher  
 478 diameter (~3 – 4  $\mu\text{m}$ ), which is due to the fact that  $dM_F/d\log D_a$  has been derived from  $dN_F/d\log$   
 479  $D_a$  assuming unit density. As observed for  $N_F$  during the month of June, the consistent morning  
 480 peak was present in  $M_F$  with only difference of prominent second peak in  $M_F$ , which starts late in  
 481 the evening at ~19:00 hr and further extends up to morning hours (~08:00 hr). Thereafter  $M_F$   
 482 concentration steadily decreased as the day progressed reaching minimum at around mid-day.

483 The early morning peak in  $M_F$  concentration was consistently observed in the size range of 3 – 4  
 484  $\mu\text{m}$  for the all the measurement months. The characteristic distribution of  $M_T$  (Fig. S8), however,  
 485 exhibited distinct behavior as compared to both  $M_F$  and  $N_T$ . The concentration peak of <1  $\mu\text{m}$   
 486 observed in  $N_T$  shifted to the higher diameter range of ~2 – 3  $\mu\text{m}$  as increase in mass is more  
 487 associated with presence of coarse mode particles. For example in June  $M_T$  exhibited similar  
 488 diurnal feature as that of  $N_T$ . The flatter trend observed in average  $M_T$  during the month of June  
 489 disappeared during the month of July and August with appearance of less prominent peak in  $M_T$   
 490 at around 12:00 hr resulting in relatively pronounced diurnal pattern (Fig. S8). The distinct  
 491 diurnal patterns of  $M_F$  and  $M_T$  showed very less relative contribution of FBAP to TAP mass as



492 compared to other observational sites (Huffman et al., 2010, 2012; Matthias-Maser and Jaenicke,  
 493 1995).

### 494 **3.3 Size distribution of particle number and mass**

495 Figure 7 shows the number and mass size distributions for TAPs and FBAPs averaged over the  
 496 entire measurement period. The TAP number size distribution,  $dN_T/d\log D_a$ , was generally broad  
 497 and dominated by a peak at the lower end of the measured size range of number size distribution  
 498 ( $D_a \approx 0.9 \mu\text{m}$ ; Fig. 7a). In  $dN_T/d\log D_a$  the concentrations exhibited a significant decrease above  
 499 diameter  $\sim 3 \mu\text{m}$  with a long tail extending on the right hand side of the distribution. The  
 500 corresponding monthly  $dN_T/d\log D_a$  are shown in Fig. S9. Overall the individual monthly  
 501  $dN_T/d\log D_a$  exhibited the similar qualitative number size distribution pattern as that of campaign  
 502 averaged TAP number size distribution. Averaged over the entire measurement period, the mass  
 503 size distribution,  $dM_T/d\log D_a$  (Fig. 7c), exhibited a broad peak at  $\sim 2.6 \mu\text{m}$  with an extended tail  
 504 to the left side of the mass size distribution, whereas on the right side a second peak started  
 505 appearing at  $D_a \approx 12 \mu\text{m}$ . The corresponding monthly averaged  $dM_T/d\log D_a$  are shown in Fig.  
 506 S10. As evident from the figure the campaign average TAP mass size distribution appeared  
 507 generally similar to each of the individual months. For accurate representation of mass size  
 508 distribution the unit-normalized mass distribution in  $D_a$  plotted in Fig. 7 (c and d) is expected to  
 509 shift to larger particle size with increased area under the curve, as  $D_a$  is directly proportional to  
 510 square root of density of the particle under consideration (Huffman et al., 2010; DeCarlo et al.,  
 511 2004).

512 The campaign average number size distribution of FBAP (Fig. 7b) exhibited monomodal shape  
 513 with much narrower peak than the TAP number size distribution, with a dominant mode at  
 514  $D_a \approx 2.8 \mu\text{m}$ , which was consistent throughout measurement period. The corresponding monthly



mean FBAP number size distributions are shown in Fig. S11. This peak was much prominent and narrow in the month of June with highest FBAP concentration and became less pronounced in July, with the lowest FBAP concentration. As reported by Huffman et al., (2010) multiple and broader peaks in  $dN_F/d\log D_a$  are most likely to originate from different sources and biological species. In the present study, however, we did not find multiple peaks in investigated FBAP number size distribution, suggesting that observed FBAPs comprised the particles from similar or same sources. The overall qualitative appearance of the average FBAP number size distribution is similar to that has been reported by previous measurements. For a semi-urban site in Central Europe Huffman et al., (2010) reported an average FBAP peak at  $3.2\ \mu\text{m}$ . Gabey et al., (2010) observed a similar peak at  $\sim 2.5\ \mu\text{m}$  at a tropical rain forest site in Borneo. From a pristine Amazonian rainforest site during wet season Huffman et al., (2012) reported a similar peak at  $\sim 2.3\ \mu\text{m}$ . For another pristine observational site in boreal forest in Finland Schumacher et al., (2013) reported a peak in FBAP number size distribution at  $\sim 3\ \mu\text{m}$ . A similar peak at  $\sim 3\ \mu\text{m}$  was also observed by Healy et al., (2014) at a rural site in Killarney national park, Ireland. This dominant peak in the range of  $2 - 3\ \mu\text{m}$  in FBAP number size distribution is strongly attributed to the fungal spores over the continent as reported by numerous previous researchers (Huffman et al., 2010, 2012; Schumacher et al., 2013; Li et al., 2011; Artaxo and Hansson, 1995; Healy et al., 2014; Gabey et al., 2010, 2013; Toprak and Schnaiter, 2013). Recently Valsan et al., (2015) investigated the morphological characteristics of PBAPs from the same site during non-monsoon season and found that fungal spores constituted the major fraction of PBAPs and nominally ranged in the size range of  $\sim 3 - 10\ \mu\text{m}$ , which roughly translates into equivalent aerodynamic diameter of  $2 - 5\ \mu\text{m}$ . The scanning electron microscopy images obtained from the filter samples occasionally collected during this field campaign showed the strong presence of variety of fungal





538 spore in the size range of 3 – 10  $\mu\text{m}$  (aerodynamic diameter 2 – 5  $\mu\text{m}$ ; discussed below; Fig. 17).  
539 As an overview of the comparison, the FBAP concentration values observed at Munnar are  
540 compared to the FBAP concentration ranges obtained using similar online measurements  
541 techniques from diverse environmental conditions across the globe, and the details are tabulated  
542 in Tab. 3. The campaign averaged FBAP mass size distribution is shown in Fig. 7d, which  
543 nominally appeared bimodal with very sharp primary peak at  $D_a \approx 3.2 \mu\text{m}$  and very broad but  
544 unappreciable second mode at  $D_a \approx 4 \mu\text{m}$ . The distinct presence of particle mass in the higher  
545 diameter range ( $>10 \mu\text{m}$ ) in FBAP mass size distribution was not prominently noticed in Munnar  
546 as compared to previously reported studies (Huffman et al., 2010; 2012). In case of TAP mass  
547 size distribution the right side tail started showing positive slope at larger diameter whereas  
548 FBAP mass size distribution consistently showed the negative slope at larger diameters. Such a  
549 distinct shape of mass size distributions for TAP and FBAP reconfirms the fact that the larger  
550 particles observed in the TAP mass distribution originated from processes that did not produce  
551 particles of the biological origin as likewise reported by Huffman et al., (2010). The  
552 corresponding monthly mean FBAP mass size distributions are shown in Fig. S12. The  
553 individual month FBAP mass size distribution exhibited the similar qualitative shape to that of  
554 average campaign. As mentioned above highest FBAP mass concentration was observed in June,  
555 which coincided with a very sharp and narrow primary peak in FBAP mass size distribution,  
556 while the lowest FBAP mass concentration during July, on the other hand, coincided with a  
557 broad primary peak with lower slope.  
558 The size-resolved ratio of FBAP to TAP averaged over the course of measurement is shown in  
559 Fig. 8 and corresponding monthly ratios are shown in Fig. S13. The relative contribution of  
560 FBAPs ( $dN_F$ ) to TAPs ( $dN_T$ ) in each size bin could be used to derive the relative contribution of



biological particles to total aerosol particles at each size. As reported by Huffman et al., (2010) the assumption of unit density of each particle implies that the value of the  $dN_F/dN_T$  ratio would invariably is equal to  $dM_F/dM_T$ . The integrated  $N_F/N_T$  and  $M_F/M_T$ , however, would have the distinct values. As can be seen from Fig. 8 and S13a considerable quantitative and qualitative difference in mean (red) and median (green) curve was consistently observed in all individual months, which likely is the result of poor counting statistics and very high variability in FBAP and TAP number concentrations. Based on the results presented by Huffman et al., (2010) the mean (red) curve, best represents the  $N_F/N_T$  ratios at the upper particle sizes; hence we will stick our further discussion about  $N_F/N_T$  ratios for the present study to the mean curve. The mean  $N_F/N_T$  ratio curves for individual months and for entire campaign exhibited two dominant peaks persistently in the particle size range  $\sim 3 - 4 \mu\text{m}$  and  $\sim 6 - 8 \mu\text{m}$ . The first prominent peak in  $dN_F/dN_T$  distribution at  $3 - 4 \mu\text{m}$  comprised  $15 - 16\%$  while the second peak at  $6 - 8 \mu\text{m}$  represented  $\sim 14 - 15\%$  of the FBAP material in TAP over the entire measurement period (Fig. 8). As can be observed from Fig. S13, the second peak in  $N_F/N_T$  ratios for July was higher ( $\sim 12\%$ ) than the first peak ( $\sim 10\%$ ) unlike other two observational months. The fact that  $N_F/N_T$  ratio is approximately zero for the particle sizes  $< 1.7 \mu\text{m}$  indicated that FBAP mainly comprised of very small fraction of submicron aerosols at Munnar. The statistics for the individual months showed that the first peak in  $dN_F/dN_T$  was more or less consistent at  $\sim 22\%$  during June and August except for the July when second peak in  $N_F/N_T$  ratios contributed more ( $\sim 12\%$ ) than the first peak ( $\sim 10\%$ ).

### 3.4 Focus periods

As described in Sec. 3.1 based on campaign overview the characteristics properties of FBAP and specifically TAP number concentration exhibited strong temporal variabilities, which could be



584 attributed to changes in prevailing meteorological conditions especially wind direction during  
585 monsoon season at Munnar. To explore the potential impact of air mass origin on number and  
586 size distribution of FBAP and TAP, we highlight three distinct focus periods:

587 1. A focus period of “dusty episode” was identified when prevailing wind was predominantly  
588 Westerly/Southwesterly and air masses mainly came from the Arabian Sea. These air masses,  
589 although almost anthropogenically clean, are laden with sea salt and dust particles during the  
590 start of the monsoon, which dominate the coarse mode fraction of atmospheric aerosols (Vinoj et  
591 al., 2014; Li and Ramanathan, 2002). These dust particles observed over this region mainly  
592 originate from West Asia, North Africa, and Arabian region (Vinoj et al., 2014). During our  
593 measurement campaign, a dusty period from 14-06-2014 00:00 hr to 25-06-2014 23:55 hr was  
594 observed and is consistent with the description given above and SEM images, which showed the  
595 presence of mineral dust, obtained during dusty period (see Sec. 3.5 below). This period was  
596 marked with an accumulated rainfall of ~1015 mm, average relative humidity of  $94.4 \pm 6.5\%$ ,  
597 average temperature of  $17.7 \pm 1.5^\circ\text{C}$ , and average wind speed  $2.8 \pm 1.3 \text{ m s}^{-1}$  (maximum wind  
598 speed of  $6.7 \text{ m s}^{-1}$ ).

599 2. A focus period of “clean period”, was observed during latter half of the monsoon season when  
600 wind direction was predominantly Westerly/Southwesterly and air masses originated over  
601 Arabian Sea. During this period, which was chosen from 09-07-2014 10:25 hr to 07-08-2014  
602 23:55 hr, FBAP and TAP concentrations were extremely low with very weak variability. This  
603 clean period was associated with persistent rainfall (accumulated rainfall of 2650 mm), average  
604 relative humidity of  $99.5 \pm 1.4\%$ , average temperature of  $16.4 \pm 0.5^\circ\text{C}$ , and average wind speed  
605  $3.7 \pm 1 \text{ m s}^{-1}$  (maximum wind speed of  $8.3 \text{ m s}^{-1}$ ).



3. A focus period of “high bio” comprised three discrete events of **high FBAP concentration** observed from 01-06-2014 09:10 hr to 05-06-2014 18:20 hr; 26-06-2014 00:05 hr to 30-06-2014 17:00 hr; and 18-08-2014 00:00 hr to 22-08-2014 08:30 hr. Interestingly this period is marked with the very distinct metrological parameters compared to the clean period: accumulated rainfall 194 mm, average relative humidity  $93.4 \pm 8.4\%$ , average temperature  $18.0 \pm 2.4^\circ\text{C}$ , and average wind speed  $1.2 \pm 0.8 \text{ m s}^{-1}$  (with maximum wind speed of  $4.6 \text{ m s}^{-1}$ ). Briefly, during “high bio” period stagnant air masses came from densely vegetated region located north of observational site, and relative humidity and temperature exhibited high variability.

#### 3.4.1 Particle number and mass concentrations

The statistical distributions of  $N_T$ ,  $N_F$ ,  $M_T$ , and  $M_F$  for three different focus periods (dusty, clean, and high bio) are shown in Fig. 9 and tabulated in Tab. 4. Each of the focus periods discussed here did not represent equal duration of the observations. The average total particle number concentration,  $N_T$ , showed a decrease of  $\sim 70\%$  from dusty period to clean period ( $\sim 4.2 \text{ cm}^{-3}$  and  $\sim 1.3 \text{ cm}^{-3}$  respectively), whereas the  $N_T$  concentration during high bio period was  $\sim 1.8 \text{ cm}^{-3}$ . The high  $N_T$  concentration during the dusty period caused the high variability between 5<sup>th</sup> and 95<sup>th</sup> percentile in  $N_T$  when averaged over entire campaign period (Fig. 3a). The fraction of dust in coarse mode aerosol, which is observed to be very high during pre-monsoon and first few days from the onset of monsoon rainfall, gradually decreased as the monsoon progressed as a result of wash out and wet deposition due to persistent rainfall in the path of air masses (Hirst 1953; Madden, 1997; Burge and Roger, 2000). The  $M_T$  exhibited similar pattern to that of  $N_T$  during three distinct focus periods with average mass concentration of  $\sim 16.3 \mu\text{g m}^{-3}$ ,  $\sim 5.1 \mu\text{g m}^{-3}$ , and  $\sim 7.7 \mu\text{g m}^{-3}$  for dusty, clean, and high bio periods, respectively.



As expected, the  $N_F$  was highest during the high bio period (Fig. 9b) with an average concentration of  $0.05 \pm 0.04 \text{ cm}^{-3}$  and high variability in higher concentration range ( $0.06 - 0.13 \text{ cm}^{-3}$ ) as evident from the distance between 75<sup>th</sup> and 95<sup>th</sup> percentile. The  $N_F$  was found to be relatively stable during the dusty period with an average concentration of  $\sim 0.02 \pm 0.008 \text{ cm}^{-3}$ . The average  $N_F$  concentration was found to be an order of magnitude lower during clean period ( $0.005 \pm 0.004 \text{ cm}^{-3}$ ) as compared to high bio period, whereas corresponding decrease in  $N_T$  from dusty to clean period ( $\sim$  by factor of 3) was not of similar magnitude. We put forward following hypothesis for such a concentration difference in  $N_F$  and  $N_T$  during three distinct periods: During clean period the predominant wind direction was Westerly/Southwesterly and air masses came from Arabian Sea bringing clean marine influx marked by persistent rainfall. As a result, the coarse mode aerosol fraction ( $N_F$  and  $N_T$ ) emitted locally were efficiently removed, however, the sea salt particles present in the air masses, which came from Arabian Sea contributed to TAP number concentration (see section 3.5). In addition to the efficient wet removal of FBAP due to persistent rainfall, the high RH level (average 99.5%), which causes the dew formation that further inhibit the spore release in turn reduced the FBAP concentration (Schumacher et al., 2013; Jones and Harrison, 2004). The mean values of  $M_F$  exhibited similar temporal trends and qualitative pattern as  $N_F$ , with highest mass concentration of  $0.58 \mu\text{g m}^{-3}$  during high bio period, which reduced by  $\sim 86\%$  ( $0.08 \mu\text{g m}^{-3}$ ) during the clean period.

As anticipated the relative contribution of FBAP in TAP during dusty and clean periods was almost negligible with  $N_F/N_T$  ratio of  $\sim 1\%$ . Whereas during the high bio period the relative FBAP number and mass contribution to corresponding TAP was  $\sim 5\%$  and  $12\%$  respectively.

#### 3.4.2 Size distribution of particle number and mass concentration



Figure 10 highlights the  $dN_F/d\log D_a$  during three distinct focus periods and corresponding  $dN_T/d\log D_a$  are shown in Fig. S14. Overall  $dN_F/d\log D_a$  exhibited pattern similar to that of campaign average.

The  $dN_F/d\log D_a$  averaged over the dusty period was dominated by a narrow peak at  $\sim 2.5 - 3.1 \mu\text{m}$ . The corresponding  $dN_F/d\log D_a$  during clean period was overall broader compared to dusty and high bio periods with gradual increase in FBAP number concentration from diameter range of  $\sim 1 - 2.3 \mu\text{m}$ , with a sharp increase thereafter, whereas downward slope exhibited the consistent pattern.  $dN_F/d\log D_a$  during high bio period exhibited relatively narrow peak at  $\sim 2.5 \mu\text{m}$ . Unlike previously reported studies (Huffman et al., 2010; 2012) the peak in  $dN_F/d\log D_a$  ( $D_a \approx 3 \mu\text{m}$ ) was not reflected in  $dN_T/d\log D_a$  mostly due to relatively less contribution of FBAP in coarse mode TAP number concentration. As can be seen from Fig. S14a the total aerosol particle number size distribution,  $dN_T/d\log D_a$ , during dusty period exhibited a peak at  $\sim 0.9 \mu\text{m}$ , with a high negative slope on the left side of the distribution curve. This peak may be comprised of mineral dust and sea salt particles, as also evident from SEM images (please refer to section 3.5) and based on the previous studies investigated aerosol composition over India during monsoon season (Vinoj et al., 2014; Moorthy et al., 1991; Vinoj and Satheesh, 2003; Satheesh and Srinivasan, 2002; Li and Ramanathan, 2002). A similar peak in  $dN_T/d\log D_a$  at  $D_a \approx 0.9 \mu\text{m}$  was observed in pristine Amazonian rainforest and particles were mostly dominated by mineral dust during high dust period (Huffman et al., 2012, Fig. 5b). During clean period  $dN_T/d\log D_a$  resembled the similar shape (peaking at  $\sim 0.9 \mu\text{m}$ ) to that of dusty period, however, with lower concentration. The corresponding  $dN_T/d\log D_a$  distribution (Fig. S14c), during high bio period, exhibited multiple peaks and appeared noisy for  $D_a < 1 \mu\text{m}$  with increasing trend in TAP number concentration for the lower diameter range of the distribution. The downward slope for  $D_a > 1 \mu\text{m}$



exhibited consistent shape (mean curve) compared to distributions observed during other two focus periods.

The FBAP mass size distribution (Fig. 11) during dusty period was dominated by bimodal peaks with prominent peak at  $\sim 3 \mu\text{m}$  and relatively less pronounced peak in the range of  $\sim 4 - 6 \mu\text{m}$  showing broader tail on the right side of the distribution curve. The  $dM_F/d\log D_a$ , during clean period, exhibited similar bimodal peaks with extended shoulder in the diameter range from  $\sim 4$  to  $7 \mu\text{m}$ . The  $dM_F/d\log D_a$  distribution during high bio period was distinct compared to two other focus periods discussed above with a prominent monomodal peak at  $\sim 3 \mu\text{m}$ . The primary peak observed in  $dM_F/d\log D_a$  in the range of  $\sim 3$  to  $4 \mu\text{m}$  was consistent during individual months and different focus periods. TAP mass size distribution (Fig. S15) exhibited similar qualitative pattern to that of campaign averaged  $dM_T/d\log D_a$  with peak between  $\sim 2.5$  to  $3.5 \mu\text{m}$  with an extended tail on the right side, which gradually increased for  $D_a > 13 \mu\text{m}$ .

The size resolved ratio of FBAP to TAP particles averaged for three distinct focus periods is shown in Fig. 12. As evident from the figure the largest fraction of FBAP particles during dusty period occurred between  $\sim 6 - 9 \mu\text{m}$  ( $\sim 20\%$ ) with relatively small contribution in the size range of  $\sim 3 - 4 \mu\text{m}$  ( $\sim 7\%$ ). The  $dN_F/dN_T$  exhibited the **sloping tails on both the sides of the distribution with steep slope on the right side**. The fact that  $N_F/N_T$  is approximately zero for the particle size range below  $\sim 1.5 \mu\text{m}$  is consistent with previous observations reported from semi urban site in central Europe and during wet season of pristine Amazonian rainforest (Huffman et al., 2010; 2012). During the clean period the maximum contribution of FBAP to TAP number concentration reduced to  $\sim 10.5\%$  in the diameter range of  $\sim 6$  to  $9 \mu\text{m}$  with another prominent, but relatively smaller contributing peak, at  $\sim 3 - 4 \mu\text{m}$  with relative contribution of  $\sim 8\%$ . During high bio period the maximum contribution of FBAP to TAP occurred between size range of  $\sim 3$



696 – 8  $\mu\text{m}$  with contribution range of  $\sim 28 - 19\%$  and relatively broad  $dN_F/dN_T$  distribution.  
 697 Interestingly during high bio period the highest contribution of FBAP to TAP number  
 698 concentration occurred at  $D_a \approx 3.5 \mu\text{m}$ , as opposed to other two focus periods when highest  
 699 contribution was observed in the larger diameter ranges of  $\sim 6 - 8 \mu\text{m}$ .  $N_F/N_T$  was consistently  
 700 found to be equal to zero for the diameter beyond  $13 \mu\text{m}$  indicating that FBAP comprised  
 701 extremely small fraction of total aerosol particles (Huffman et al., 2010; 2012). The two  
 702 prominent peaks observed during focus periods were clearly evident in campaign-averaged  
 703  $dN_F/dN_T$  (Fig. 8; peaks at  $\sim 3.5$  and  $6 \mu\text{m}$ ).

### 704 3.4.3 Diurnal patterns

705 A prominent early morning peak in  $N_F$  during high bio period in the diameter range of  $1.5 - 3$   
 706  $\mu\text{m}$  was observed from 06:00 hr to 08:00 hr, which clearly reflected in campaign averaged  
 707 diurnal patterns at the same hour of the day. The diurnal variations in  $N_F$  during dusty and clean  
 708 periods were not so pronounced (Fig. 13) as compared to the variations during high bio period.  
 709 During dusty period  $N_F$  showed slightly high concentration starting from  $\sim 20:00$  hrs and  
 710 persistently remained high until early morning without any variations, whereas during clean  
 711 period  $N_F$  concentration consistently remained flat throughout 24 hrs. The evening peak  
 712 observed during dusty period, however, was clearly absent during high bio period. A moderately  
 713 pronounced peak in  $N_F$  during evening hours at  $\sim 20:00$  hr during dusty periods might indicate  
 714 that releasing mechanism of bioaerosols was efficient as a result of nocturnal sporulation. This  
 715 can further imply that the morning and late evening peaks in  $dN_F/d\log D_a$  at  $D_a \approx 3 \mu\text{m}$  most likely  
 716 resulted from different type of spores (Hirst, 1953). As listed by Huffman et al., (2012) the  
 717 emission and dispersal of bioaerosols is strongly coupled with environmental variables such as  
 718 solar radiation, temperature, and relative humidity and each of these variables have strong





719 diurnal cycles. It has been well documented that relative humidity, in particular, plays an  
 720 important role in active wet discharge of fungal spores (Adhikari et al., 2006; Burch and Levetin,  
 721 2002; Elbert et al., 2007; Jones and Harrison, 2004; Quintero et al., 2010; Zhang et al., 2010) ,  
 722 which constitutes major fraction of atmospheric bioaerosols (Ansari et al., 2015; Bauer et al.,  
 723 2008; Bowers et al., 2013; Fröhlich-Nowoisky et al., 2009; Sesartic and Dallafior, 2011;  
 724 Spracklen and Heald, 2014). The meteorological parameters exhibited pronounced diurnal  
 725 variations during high bio period, where RH decreased to a level ( $\sim 60 - 80\%$ ), which is  
 726 considered to be favorable for release of the fungal spores (Jones and Harrison, 2004; Santarpia  
 727 et al., 2013). During dusty and clean period the persistence of high RH values in the range of  $\sim 90$   
 728  $- 100\%$ , however, might have inhibited the active wet discharge of fungal spore (Schumacher et  
 729 al., 2013; ) thus resulting the weak diurnal variation in  $N_F$ . Unlike  $N_F$ ,  $N_T$  remained flat without  
 730 any pronounced diurnal variations during three distinct focus periods (Fig. S16). The  
 731 corresponding diurnal cycle of FBAP mass concentration and size distributions for three focus  
 732 periods are shown in Fig. S17.  $M_F$  exhibited similar diurnal patterns to that of  $N_F$  during three  
 733 focus periods.  $M_T$  as like  $N_T$  remained flat during dusty period, however exhibited slightly  
 734 pronounced diurnal pattern during clean and high bio period between 09:00 hrs and 16:00 hrs  
 735 (Fig. S18).

### 736 **3.5 SEM images**

737 Figure 14 shows the exemplary SEM images of biological particle types often observed during  
 738 the SW monsoon season at Munnar. The details about the sampling techniques, instrument used,  
 739 etc. for obtaining these bioaerosol images are discussed in details by Valsan et al., (2015). Note  
 740 that these images are not being presented here for any quantitative purpose and to draw any  
 741 specific scientific conclusions but mainly to showcase the particle types consistently observed



742 throughout the measurement period. As seen from the SEM images majority of the particles are  
743 mostly likely fungal spores. Based on their distinct morphology the spores in Fig. 14a-c most  
744 likely appeared to be of Basidiospores. The appearance of small protuberances on the surface  
745 suggests that the spore in Fig. 14a most likely belonged to the *Hydnaceae* family (Grand and  
746 Vandyke, 1976; Valsan et al., 2015). The Basidiospores shown in Fig. 14b and c were seen in  
747 abundance in all the samples collected during the campaign. Some of the spores observed  
748 appeared to be coated with salt particles (Fig 14e) and might have been carried from a distant  
749 source by the SW monsoon winds. The spores shown in Fig 14 (d and f) most likely appeared to  
750 be spores of Ascomycota division. The particle shown in Fig. 14g was most likely a mineral dust  
751 particle sampled during high dusty episode. Similar particles of varying size during dusty  
752 episode were consistently observed during SEM analysis. Fig 14h and i shows the images of the  
753 typical sea salt particles observed during samples collected at Munnar during measurement  
754 campaign when wind predominantly came from Westerly/Southwesterly direction travelling over  
755 Indian Ocean and Arabian Sea.

### 756 **3.6 Meteorological Correlations**

757 The results obtained with UV-APS data analysis during the campaign at Munnar were plotted  
758 with respect to meteorological parameters to investigate factors responsible for bioaerosol  
759 release and their variations in the atmosphere.

#### 760 *Impact of wind direction*

761 The wind rose diagrams scaled by  $N_F$ ,  $D_g$ , and  $D_{g,T}$  were also prepared for entire measurement  
762 period and three distinct focus periods. These plots are in a way similar to the traditional wind  
763 rose diagram (Fig. S19) except, instead of wind speed, they are scaled by characteristic FBAP



and TAP parameters, which indicate the frequency of occurrence of respective parameter with respect to wind direction (Sherman et al., 2015). As can be seen from Fig. S19, predominant wind direction during entire campaign was Westerly/Southwesterly with frequency of occurrence of about ~90%. The wind speed broadly ranged between  $2 - 5 \text{ m s}^{-1}$  with no prominent diurnal variations. The overall wind direction and back trajectory analysis (Fig. 1) shows that the sampled air masses may have had their origin over the Indian Ocean thereafter turning eastward after crossing the equator and travelling several hundred kilometers over Arabian Sea before reaching the observational site (Fig. 1). The predominant wind pattern during dusty (>95% frequency of occurrence;  $2 - 6 \text{ m s}^{-1}$ ) and clean periods (~100 frequency of occurrence;  $2 - 6 \text{ m s}^{-1}$ ) was Westerly/Southwesterly. Whereas during high bio period only ~50% of the time winds came from Westerly/Southwesterly direction and rest comprised the stagnant and calm ( $0 - 2 \text{ m s}^{-1}$ ) winds from all other directions with highest contribution of northerly winds (Fig. S19).

Wind rose diagram scaled by FBAP number concentration is shown in Fig. 15. During the entire campaign the predominant wind showed that ~85% of the time FBAP concentration occurred in the range of  $0 - 0.05 \text{ cm}^{-3}$  (Fig. 15a) occasionally exceeding  $0.05 \text{ cm}^{-3}$  and was contributed by Westerly/Southwesterly winds. The occurrence of relatively low FBAP concentration during entire campaign is consistent with low concentration occurrence during dusty ( $0 - 0.05 \text{ cm}^{-3}$ ; >90% frequency of occurrence) and clean ( $<0.01 \text{ cm}^{-3}$ ; ~90% frequency of occurrence) periods. During high bio period the FBAP concentration,  $>0.05 \text{ cm}^{-3}$  exhibited ~40% frequency of occurrence of which ~50% was contributed by predominant wind from North and Northwest.

Similarly the wind rose diagram scaled by geometric mean diameter ( $D_g$ ) of  $dN_F/d\log D_a$ , is shown in Fig. 16. The average size of the FBAP particles associated with Westerly/Southwesterly winds when analyzed for entire the campaign ranged between  $2 - 4 \mu\text{m}$



787 of which ~65% of the time  $D_g$  was observed to be  $\leq 3 \mu\text{m}$ . During three distinct focus periods the  
788 frequency of occurrence of FBAP particles in the higher size range ( $3 - 4 \mu\text{m}$ ) was strongly  
789 associated with the Westerly/Southwesterly winds (Figs. 16b – d). The corresponding wind rose  
790 diagram scaled by geometric mean diameter of  $dN_T/d\log D_a(D_{g,T})$  is shown in Fig. S20. During  
791 entire measurement campaign the frequency of occurrence of  $D_{g,T}$  in the size range of  $0.8 - 0.9$   
792  $\mu\text{m}$  was ~70% and was mostly associated with Westerly/Southwesterly winds. During dusty  
793 period particles in the size range of  $0.8 - 0.9 \mu\text{m}$  diameter contributed for >95% frequency of  
794 occurrence for the entire size range, whereas during clean period ~20% occurrence of the  
795 particles in the size range other than  $0.8 - 0.9 \mu\text{m}$  were also observed. On the other hand during  
796 high bio period total particles in the size range  $0.5 - 0.8 \mu\text{m}$  were observed with ~50% frequency  
797 of occurrence constituted by varying wind patterns mostly dominated by northerly winds.

798 The FBAP concentration exhibited strong dependence on the wind direction for this  
799 observational site. During the high bio period the increase in frequency of occurrence of FBAP  
800 number concentrations  $>0.1 \text{ cm}^{-3}$  coincided with **stagnant wind** coming from North and  
801 Northwest (Fig. 17a). During high bio period, as like dusty and clean periods the predominant  
802 wind pattern was Westerly/Southwesterly, however, with relatively low frequency of occurrence  
803 as compared to other two periods. To have the better understanding of relative contribution of  
804 wind direction in high FBAP number concentration during high bio period, we prepared the  
805 separate wind rose diagrams for FBAP concentration  $>0.1 \text{ cm}^{-3}$  and  $<0.1 \text{ cm}^{-3}$  as shown in Fig.  
806 17. The FBAP number concentration  $>0.1 \text{ cm}^{-3}$  was associated with **calm ( $0 - 1 \text{ m s}^{-1}$ ; ~80%**  
807 **frequency of occurrence) and predominant Northerly winds** (Fig. 17a) as opposed to high wind  
808 speed ( $2 - 5 \text{ m s}^{-1}$ ) and predominant Westerly/Southwesterly winds for the FBAP number  
809 concentration  $<0.1 \text{ cm}^{-3}$  (Fig. 17b). The calm **northerly winds** coming over from densely



810 vegetated regions in combination with local FBAP sources during high bio period could be the  
811 strong reason for the built up resulting in higher FBAP number concentration during this  
812 episode, whereas, Westerly/Southwesterly winds were consistently marked by very low FBAP  
813 number concentration mostly owing to higher wind speeds. Further, it might also due to the fact  
814 that the air masses arriving at observational site originated over cleaner marine region, which  
815 may be potential but weak source of bioaerosols combined with possible wash out/wet  
816 deposition due to persistent rainfall during the transport. Nominally the frequency of occurrence  
817 of larger particles ( $3 - 4 \mu\text{m}$ ) during Westerly/Southwesterly winds was high compared to the  
818 Northerly winds, where particles were mostly of smaller size ( $1 - 3 \mu\text{m}$ ). We hypothesize that  
819 during Northerly wind the bioaerosols were mostly comprised of Basidiospores, which is  
820 consistent with SEM images obtained during measurement period. Frohlich-Nowoisky et al.,  
821 (2012) reported that, region with dominant prevalence of marine air masses have larger  
822 proportions of Ascospores and in contrast, the continental air masses exhibit higher proportions  
823 of Basidiospores. However, due to technical difficulties associated with sampling we could not  
824 establish the fact that spores observed at this observational site during Westerly/Southwesterly  
825 winds were dominated by Ascospores and these details will be addressed in follow up studies.  
826 The corresponding wind rose scaled by  $D_{g,T}$  obtained from  $dN_T/d\log D_a$  is shown in Fig. S21.

827 As shown in Tab. 5 the wind speed was observed to be negatively affecting the  $N_F$  during entire  
828 measurement period and is consistent with previously reported studies (Hameed et al., 2012;  
829 Almaguer et al., 2013; Lyon et al., 1984; Quintero et al., 2010). The increased  $N_F$  concentration  
830 levels during calm and stagnant wind might indicate that observed bioaerosols were dominated  
831 by the local source rather than transported from longer distances (Sadys et al., 2014; Hara and  
832 Zhang, 2012; Bovallius et al., 1978; Maki et al., 2013; Prospero et al., 2005; Creamean et al.,



2013) as lower wind speed may actually increase emission of some specific type of spores  
(Huffman et al., 2012; Jones and Harrison, 2004; Troutt and Levetin, 2001; Kurkela, 1997).

### 3.6.1 Correlation with relative humidity and temperature

Correlation coefficient derived between  $N_F$  and relative humidity averaged over the entire campaign is shown in Fig. 18 and corresponding  $R^2$  values for three distinct focus periods are shown in Tab. 5. In general an increase in  $N_F$  concentration with increasing relative humidity was observed with moderate correlation coefficient ( $R^2=0.58$ ). Depending upon the type of bioaerosols, geographical location, and local climate,  $N_F$  has shown varied dependence on relative humidity and precise response of the spore concentration to relative humidity is difficult to characterize. For example number of studies have shown that spores of genus like *Cladosporium*, *Alternaria*, and *Epiccocum* are known to exhibit the negative correlation with relative humidity (Oliveira et al., 2010; Herrero et al., 1996; Kurkela, 1997; Oh et al., 1998; Healy et al., 2014) on the other hand studies have also found these spores to be positively correlated with relative humidity (Quintero et al., 2010; Hjelmroos, 1993; Ho et al., 2005). Whereas genus like *Ustilago* and some other Basidiospores may as well exhibit strong positive correlation with relative humidity (Sabariego et al., 2000; Quintero et al., 2010; Ho et al., 2005; Calderon et al., 1995). Further, Ascospores concentrations are known to increase during and after rainfall (Burch and Levetin, 2002; Elbert et al., 2007; Hasnain, 1993; Hirst, 1953; Toutt and Levetin, 2001; Lyon et al., 1984; Oh et al., 1998) whereas Basidiospores exhibited a strong resemblance to the diurnal pattern of relative humidity (Li and Kendrick 1994; Hasnain 1993; Tarlo et al., 1979; Trout and Levetin 2001). Almaguer et al., (2013) have reported that in tropical region relative humidity has greater influence than temperature on the airborne spore counts and may be a pre-requisite for release of spores (Hollins et al., 2004). Thus, the combination of



856 persistent threshold relative humidity (~60 – 95% as reported by Ho et al., 2005) and rainfall can  
 857 cause the increase in the spore concentration and the excessive and persistent rain, however,  
 858 tends to wash the spore out of the atmosphere further reducing their concentration levels (Burge  
 859 1986; Horner et al., 1992; Troutt and Levetin, 2001). Based on these arguments combined with  
 860 observed meteorological conditions we expect that the bioaerosols reported here from Munnar  
 861 mainly consisted of Basidiospores during the SW monsoon season as also evident from SEM  
 862 images (discussed above). This is consistent with results reported by Valsan et al., (2015) where  
 863 they found the dominant presence of dry air spora (*Cladosporium*) during relatively dry and  
 864 warm weather from the same observational site. In general,  $N_F$  and  $N_F/N_T$  decreased with  
 865 increasing wind speed ( $R^2=0.6$  and  $R^2=0.78$ , respectively) indicating that wind speed may be one  
 866 of the strong factors for observed high  $N_F$  concentrations at this site. As compared to previously  
 867 reported correlation between  $N_F$  and meteorological parameters (Santarpia et al., 2013), the  
 868 relations shown for this observational site appeared to be more robust and conclusive. For  
 869 example since the variability derived in  $N_T$  ( $N_T - N_{T,min} / N_{T,max} - N_{T,min}$ ; not shown here) was more  
 870 consistent and high as compared to variability derived in  $N_F$  ( $N_F - N_{F,min} / N_{F,max} - N_{F,min}$ ), which  
 871 was more episodic and hence one would expect the weak correlation between  $N_T$  and  
 872 meteorological parameters (Tab. 5).

873 On the other hand several studies have reported that in temperate regions temperature is probably  
 874 the most important meteorological parameter affecting the spore concentration (Levetin and  
 875 Horner, 2002; Adhikari et al., 2006) with highest spore concentration during summer season  
 876 (Emberlin et al., 1995; Hasnain, 1993; Herrero et al., 1996; Hjelmroos, 1993; Li et al., 2011;  
 877 Schumacher et al., 2013). When the relation between temperature and spore concentration was  
 878 investigated on averaged diurnal basis, however, spore concentration have been observed to



879 decrease with the increasing temperature (Burch and Levetin, 2002; Calderon et al., 1995;  
880 Sabariego et al., 2000; Schumacher et al., 2013; Trejo et al., 2013). Consistent with this trend, we  
881 have found significant negative correlation between  $N_F$  and temperature ( $R^2=0.65$ ) averaged over  
882 the entire measurement period at Munnar. The correlation coefficient between  $N_F$  and  
883 temperature for three distinct focus periods is given in Tab. 5. The correlation coefficient  
884 between  $N_F/N_T$  and meteorological parameters in general yielded higher  $R^2$  values. Note,  
885 however, that the interpretation presented here based on the correlation analyses performed  
886 between  $N_F$  and meteorological parameters were intended not to generalize and extrapolate  
887 conclusions to various other ecosystems (including Indian region) and different seasons of the  
888 year (including non-monsoon in India) but were presented to take an opportunity to formulate  
889 preliminary hypothesis about role of meteorological parameters in governing the variabilites of  
890 bioaerosls specific to this observational site for the monsoon season only.

#### 891 **4 Summary and Conclusions**

892 During these maiden online measurements of biological aerosol particles we operated a UV-APS  
893 continuously during the SW monsoon season (1.June – 21.August) of 2014 at a high-altitude site  
894 of Munnar in Western Ghats in Southern tropical India. The number and mass size distributions  
895 and corresponding concentrations of biological aerosol were quantified for three distinct focus  
896 periods namely dusty period, high-bio period, and clean period identified based on the prominent  
897 wind direction. We have analyzed the three month time series of integrated coarse particle  
898 number and mass concentrations, as well as particle number and mass size distributions of both,  
899 the total and fluorescence biological aerosol particles. Over the course of entire measurement  
900 period the coarse particle number concentration of FBAPs varied in the range of  $0.2 \times 10^{-3} \text{ cm}^{-3}$   
901 to  $0.63 \text{ cm}^{-3}$  with an arithmetic mean value of  $0.02 \text{ cm}^{-3}$  ( $\pm 0.02 \text{ cm}^{-3}$ ). This average concentration





902 accounted for 0.04 – 53% (mean value  $2.1\% \pm 4.05\%$ ) of the total coarse particle number  
903 concentration. The coarse particle mass concentrations of FBAPs varied in the range of  $0.5 \times 10^{-3}$   
904  $- 4.93 \mu\text{g m}^{-3}$  with an arithmetic mean ( $\pm$ standard deviation) value of  $0.24 (\pm 0.28) \mu\text{g m}^{-3}$ .

905 The average FBAP concentration during the entire measurement period was found to be highest  
906 in June ( $0.03 \text{ cm}^{-3}$ ) and lowest in July ( $0.007 \text{ cm}^{-3}$ ). The FBAP concentrations observed at  
907 Munnar during SW monsoon season are within the range but slightly on the lower side of the  
908 bioaerosol concentrations reported by previous researchers using various online and offline  
909 techniques. Numerous other studies from different part of the world have reported detailed  
910 description about observed biological aerosol particle number concentrations using offline and  
911 online techniques from various environments (Despres et al., 2007; Huffman et al., 2010, 2012;  
912 Adhikari et al., 2004; Bovallius et al., 1978; Bowers, et al., 2009, 2013; Lee et al., 2010;  
913 Matthias-Maser and Jaenicke, 1995; Matthias-Maser et al., 2000; Shaffer and Lighthart, 1997;  
914 Tong and Lighthart, 1999; Wang et al., 2007; Li et al., 2011; Hameed et al., 2009; Bauer et al.,  
915 2008; Schumacher et al., 2013; Gabey et al., 2010, 2011, 2013; Saari et al., 2015; Toprak and  
916 Schnaiter, 2013; Healy et al., 2014). For brevity, here we compare the number concentrations  
917 observed at Munnar only with number concentrations from varying environments reported by  
918 previous researchers using online measurements. Huffman et al., (2010) have reported coarse  
919 mode average FBAP number concentration from four months of measurement to be  $0.03 \text{ cm}^{-3}$ ,  
920 which constituted ~4% of total coarse mode particles from a semi-urban site of Mainz in Central  
921 Europe. The median FBAP concentration during the wet season of pristine tropical Amazonian  
922 rainforest region was found be  $0.07 \text{ cm}^{-3}$ , which constituted ~24% of total coarse mode particle  
923 number concentration (Huffman et al., 2012). By analyzing the full one-year observations from  
924 Boreal forest in Hyytiala and pine forest in Colorado, Schumacher et al., (2013) reported highest



925 FBAP concentration in summer of  $0.046 \text{ cm}^{-3}$  (constituting ~13% of total coarse mode particles)  
926 and  $0.03 \text{ cm}^{-3}$  (constituting ~8.8% of total coarse mode particles), respectively. Healy et al.,  
927 (2014) reported the average FBAP concentration of  $\sim 0.01 \text{ cm}^{-3}$  using the UV-APS measurements  
928 carried out with in the Killarney national park, Kerry situated in Southwest of Ireland. Gabey et  
929 al., (2013) by performing the measurements at a high altitude cite in central France reported  
930 averaged FBAP concentration of  $0.012 \text{ cm}^{-3}$  and  $0.095 \text{ cm}^{-3}$  using two-wavelength (280 nm and  
931 370 nm respectively) single-particle UV-induced fluorescence spectrometer. Gabey et al., (2010)  
932 from tropical rainforest in Borneo, Malaysia reported that mean FBAP number fraction in the  
933 size range of  $0.8 - 20 \mu\text{m}$  was ~55% and ~28% below and above the forest canopy, respectively.  
934 It is important to note, however, that the measurement results compared here were obtained from  
935 different instrumentation operating with different wavelength. Nevertheless, the FBAP number  
936 concentrations observed under various environmental conditions are largely comparable to the  
937 FBAP number concentration observed at Munnar during SW monsoon season. Note that the  
938 relative contribution of FBAP number concentration to total coarse mode particles may show a  
939 strong spatial variability.

940 The average observed  $dN_F/d\log D_a$  exhibited a peak at  $\sim 3 \mu\text{m}$ , which was consistent even during  
941 distinct focus periods with slight quantitative variation in the FBAP number concentration. Such  
942 a consistency in the peak of  $dN_F/d\log D_a$  during entire measurement period is an indication of the  
943 fact that sources and type of bioaerosols did not exhibit considerable variability and diversity at  
944 Munnar during SW monsoon season. The peak observed in  $dN_F/d\log D_a$  in this study is  
945 consistent with range of the peaks published by previous researchers. At a semi-urban site in  
946 Central Europe the peak in  $dN_F/d\log D_a$  was observed at  $\sim 3 \mu\text{m}$  (Huffman et al., 2010). In  
947 pristine tropical rainforest region of Amazonia a peak in  $dN_F/d\log D_a$  was found at  $\sim 2.5 \mu\text{m}$



948 (Huffman et al., 2012). Whereas the peak in  $dN_F/d\log D_a$  at a boreal forest in Finland exhibited a  
949 strong seasonal dependence with different modes at  $\sim 1.5 \mu\text{m}$ ,  $\sim 3 \mu\text{m}$ , and  $\sim 5 \mu\text{m}$  indicating  
950 differences in the bioaerosol sources (Schumacher et al., 2013). In the pine forest of Colorado the  
951 distinct peaks were observed at  $\sim 1.5 \mu\text{m}$  and  $\sim 5 \mu\text{m}$  (Schumacher et al., 2013). The mode at  $\sim 3$   
952  $\mu\text{m}$  is likely due to the fungal spore whose release mechanism is strongly governed by the  
953 combination of relative humidity and temperature (Huffman et al., 2010 and references therein).

954 On the diurnal scale a pronounced diurnal cycle with  $\sim 3 \mu\text{m}$  peak with a maximum concentration  
955 at  $\sim 06:00$  hr was observed when averaged over entire measurement period. This general pattern  
956 is consistent with previous studies reporting the early morning peak in FBAP concentration for  
957 various environmental conditions (Healy et al., 2014; Huffman et al., 2012; Schumacher et al.,  
958 2013; Toprak and Schnaiter, 2013). The early morning peak, which in the present case appears to  
959 be strongly governed by the diurnal variations in relative humidity, is most likely to be  
960 contributed by Basidiospores as their release in the atmosphere is strongly coupled with relative  
961 humidity (Adhikari et al., 2006; Burch and Levetin, 2002; Hasnain, 1993; Healy et al., 2014; Ho  
962 et al., 2005; Huffman et al., 2012). This is also consistent with the SEM images shown and  
963 discussed above.

964 The meteorological parameters were observed to correlate significantly with FBAP concentration  
965 at Munnar. When investigated on a daily averaged basis (24 hr), however, no significant  
966 correlation between  $N_F$  and meteorological parameters except moderate negative correlation with  
967 precipitation was observed. During the entire measurement campaign, except on few occasions  
968 no significant variations in temperature and relative humidity was observed. This in combination  
969 with persistent rainfall resulting in the wash out/wet deposition of biological aerosol particles  
970 might have caused such a weak correlation for a daily averaged (24 hr) analysis. On a diurnal



scale, however, a significant correlation between  $N_F$  and meteorological parameters was observed. We observed that  $N_F$  followed the similar diurnal trend to that of relative humidity and was anti-correlated with temperature. As reported by previous studies from selected locations (Huffman et al., 2013; Schumacher et al., 2013; Prenni et al., 2013; Hirst 1953) we did not observe any sharp increase in  $N_F$  concentration immediately after or during rainfall. We hypothesize that the spore built-up and release of certain species can happen only at certain threshold relative humidity (Jones and Harrison, 2004). Under the dry environmental conditions where relative humidity levels rarely attain such threshold required for fungal spore release can cause the strong built up of fungal spores inside fungal bodies. Under these conditions precipitation can cause the relative humidity levels to increase up to threshold required for fungal spore release in combination with mechanical splashing due to raindrops, and can cause the sudden and sharp increase in spore concentrations. On the contrary, like in present case, the incessant persistence of high humidity conditions can cause the continuous release of the spore without an opportunity for built-up of fungal spores in fungal body to be released during rainfall. It is also reported that persistent high levels of relative humidity can inhibit the sporulation (Schumacher et al., 2013) further considerably reducing the spore release. The correlation between  $N_F$  and wind speed was found to be strongly negative. Since majority of the spore release was dominated by the local sources, the strong winds coming over from West/Southwest direction, which were relatively clean, might have caused the dilution of air mass thus reducing the spore concentration.

Overall, the long-term measurements reported in this manuscript showed the quantitative and qualitative agreement with previously reported studies. The emissions and abundance of biological aerosol particles in Western Ghats air during monsoon season appeared to be closely



linked to the variabilities in the meteorological parameters. As reported by Huffman et al., (2012) and corroborated by the observations reported in this study, UV-APS is successfully able to detect the aerosol particles of biological origin, however, may pose certain limitations in scientific interpretation from the obtained data. The scatter plot analysis carried out between  $N_F$  and  $N_T$  for submicron and supermicron particles indicated that submicron particles at this observational site were also dominated by aerosol particles of biological origin, thus indicating the lowest possible interference from particles of anthropogenic origin known to exhibit the fluorescence at the prescribed wavelength used in UV-APS. Hence, given observational site can be termed as relatively pristine while under the influence of SW monsoon season. The contrasting characteristics of this observational site associated with pollution and interference of non-biological aerosol particles in fluorescence will be discussed in follow up studies. We propose and intend to take forward these studies by means of performing simultaneous online measurements of biological aerosol particle number concentrations in high time and size resolution under contrasting environments during distinct meteorological seasons over Indian region. This future work could be supplemented with advanced offline measurement techniques including SEM analysis, DNA analysis, and fluorescence microscopy of the samples collected in parallel with the measurements. We believe that such a comprehensive approach over Indian region would be helpful in understanding the possible tight coupling between aerosol and hydrological cycle especially during monsoon. This could also help to better understand the implication of biological aerosols on crops and human health where agricultural industry has the major share in GDP to cater the need of 18% of the world's total population.

#### **Acknowledgement:**



SSG acknowledge the combined financial support from Max Planck Society and Department of Science and Technology, Government of India under the Max Planck Partner Group Program. Authors are thankful to Akila M, Hema P, Shika S, Aleena, Hasitha, Reshma, Sanu, and Tabish U. Ansari for their support in planning, execution, and completion of the measurement campaign. Authors thankfully acknowledge the support from Gerhard Lammel, Multiphase Chemistry Department, Max Planck Institute for Chemistry for his support during campaign and providing the meteorological data for comparison. Authors are grateful to the Sophisticated Analytical Instrument Facility (SAIF), IIT Madras for making SEM available for morphological analysis. Authors gratefully acknowledge US Geological Survey for the topography data in DEM format and NOAA ARL for providing HYSPLIT air mass back trajectory calculations.

## References:

- Adhikari, A., Sen, M. M., Gupta-Bhattacharya, S., and Chanda, S.: Air-borne viable, non-viable, and allergenic fungi in a rural agricultural area of India: a 2-year study at five outdoor sampling stations, *Science of the Total Environment*, 326, 123-141, 10.1016/j.scitotenv.2003.12.007, 2004.
- Adhikari, A., Reponen, T., Grinshpun, S. A., Martuzevicius, D., and LeMasters, G.: Correlation of ambient inhalable bioaerosols with particulate matter and ozone: A two-year study, *Environmental Pollution*, 140, 16-28, 10.1016/j.envpol.2005.07.004, 2006.
- Agranovski, V., Ristovski, Z., Hargreaves, M., Blackall, P. J., and Morawska, L.: Performance evaluation of the UVAPS: influence of physiological age of airborne bacteria and bacterial stress, *Journal of Aerosol Science*, 34, 1711-1727, 10.1016/s0021-8502(03)00191-5, 2003.
- Agranovski, V., Ristovski, Z. D., Ayoko, G. A., and Morawska, L.: Performance evaluation of the UVAPS in measuring biological aerosols: Fluorescence spectra from NAD(P)H coenzymes and riboflavin, *Aerosol Sci. Technol.*, 38, 354-364, 10.1080/02786820490437505, 2004.
- Agranovski, V., and Ristovski, Z. D.: Real-time monitoring of viable bioaerosols: capability of the UVAPS to predict the amount of individual microorganisms in aerosol particles, *Journal of Aerosol Science*, 36, 665-676, 10.1016/j.jaerosci.2004.12.005, 2005.
- Almaguer, M., Aira, M.-J., Rodríguez-Rajo, F. J., and Rojas, T. I.: Temporal dynamics of airborne fungi in Havana (Cuba) during dry and rainy seasons: influence of meteorological parameters, *International Journal of Biometeorology*, 58, 1459-1470, 10.1007/s00484-013-0748-6, 2013.
- Andreae, M. O., and Rosenfeld, D.: Aerosol-cloud-precipitation interactions. Part 1. The nature and sources of cloud-active aerosols, *Earth Science Reviews*, 89, 13-41, 2008.
- Ansari, T. U., Valsan, A. E., Ojha, N., Ravikrishna, R., Narasimhan, B., and Gunthe, S. S.: Model simulations of fungal spore distribution over the Indian region, *Atmospheric Environment*, 122, 552-560, <http://dx.doi.org/10.1016/j.atmosenv.2015.10.020>, 2015.
- Artaxo, P., and Hansson, H. C.: Size distribution of biogenic aerosol-particles from the Amazon basin, *Atmospheric Environment*, 29, 393-402, 10.1016/1352-2310(94)00178-n, 1995.



- 1053 Bauer, H., Schueller, E., Weinke, G., Berger, A., Hitznerberger, R., Marr, I. L., and Puxbaum, H.:  
1054 Significant contributions of fungal spores to the organic carbon and to the aerosol mass balance  
1055 of the urban atmospheric aerosol, *Atmospheric Environment*, 42, 5542-5549,  
1056 10.1016/j.atmosenv.2008.03.019, 2008.
- 1057 Bhati, H. S., and Gaur, R. D.: Studies on Aerobiology - Atmospheric fungal spores, *New*  
1058 *Phytologist*, 82, 519-527, 10.1111/j.1469-8137.1979.tb02678.x, 1979.
- 1059 Bovallius, A., Bucht, B., Roffey, R., and Anas, P.: 3-Year investigation of natural airborne  
1060 bacterial-flora at 4 localities in Sweden, *Applied and Environmental Microbiology*, 35, 847-852,  
1061 1978.
- 1062 Bowers, R. M., Lauber, C. L., Wiedinmyer, C., Hamady, M., Hallar, A. G., Fall, R., Knight, R.,  
1063 and Fierer, N.: Characterization of Airborne Microbial Communities at a High-Elevation Site  
1064 and Their Potential To Act as Atmospheric Ice Nuclei, *Applied and Environmental*  
1065 *Microbiology*, 75, 5121-5130, 10.1128/aem.00447-09, 2009.
- 1066 Bowers, R. M., Clements, N., Emerson, J. B., Wiedinmyer, C., Hannigan, M. P., and Fierer, N.:  
1067 Seasonal Variability in Bacterial and Fungal Diversity of the Near-Surface Atmosphere,  
1068 *Environmental Science & Technology*, 47, 12097-12106, 10.1021/es402970s, 2013.
- 1069 Brosseau, L. M., Vesley, D., Rice, N., Goodell, K., Nellis, M., and Hairston, P.: Differences in  
1070 detected fluorescence among several bacterial species measured with a direct-reading particle  
1071 sizer and fluorescence detector, *Aerosol Sci. Technol.*, 32, 545-558, 10.1080/027868200303461,  
1072 2000.
- 1073 Burch, M., and Levetin, E.: Effects of meteorological conditions on spore plumes, *International*  
1074 *Journal of Biometeorology*, 46, 107-117, 10.1007/s00484-002-0127-1, 2002.
- 1075 Burge, H. A.: Some comments on the aerobiology of fungus spores, *Grana*, 25, 143-146, 1986.
- 1076 Burge, H. A., and Rogers, C. A.: Outdoor allergens, *Environmental Health Perspectives*, 108,  
1077 653-659, 10.2307/3454401, 2000.
- 1078 Burrows, S. M., Butler, T., Jöckel, P., Tost, H., Kerkweg, A., Pöschl, U., and Lawrence, M. G.:  
1079 Bacteria in the global atmosphere - Part 2: Modeling of emissions and transport between  
1080 different ecosystems, *Atmos. Chem. Phys.*, 9, 9281-9297, 2009.
- 1081 Calderon, C., Lacey, J., McCartney, H. A., and Rosas, I.: Seasonal and diurnal-variation of  
1082 airborne basidiomycete spore concentrations in Mexico-city, *Grana*, 34, 260-268, 1995.
- 1083 Chakraborty, P., Gupta-Bhattacharya, S., Chakraborty, C., Lacey, J., and Chanda, S.: Airborne  
1084 allergenic pollen grains on a farm in West Bengal, India, *Grana*, 37, 53-57, 1998.
- 1085 Coz, E., Artinano, B., Clark, L. M., Hernandez, M., Robinson, A. L., Casuccio, G. S., Lersch, T.  
1086 L., and Pandis, S. N.: Characterization of fine primary biogenic organic aerosol in an urban area  
1087 in the northeastern United States, *Atmospheric Environment*, 44, 3952-3962,  
1088 10.1016/j.atmosenv.2010.07.007, 2010.





- 1089 Creamean, J. M., Suski, K. J., Rosenfeld, D., Cazorla, A., DeMott, P. J., Sullivan, R. C., White,  
1090 A. B., Ralph, F. M., Minnis, P., Comstock, J. M., Tomlinson, J. M., and Prather, K. A.: Dust and  
1091 Biological Aerosols from the Sahara and Asia Influence Precipitation in the Western U.S,  
1092 Science, 339, 1572-1578, 10.1126/science.1227279, 2013.
- 1093 DeCarlo, P. F., Slowik, J. G., Worsnop, D. R., Davidovits, P., and Jimenez, J. L.: Particle  
1094 morphology and density characterization by combined mobility and aerodynamic diameter  
1095 measurements. Part 1: Theory, Aerosol Sci. Technol., 38, 1185-1205, 2004.
- 1096 DeLeon-Rodriguez, N., Lathem, T. L., Rodriguez-R, L. M., Barazesh, J. M., Anderson, B. E.,  
1097 Beyersdorf, A. J., Ziemba, L. D., Bergin, M., Nenes, A., and Konstantinidis, K. T.: Microbiome  
1098 of the upper troposphere: Species composition and prevalence, effects of tropical storms, and  
1099 atmospheric implications, Proceedings of the National Academy of Sciences of the United States  
1100 of America, 110, 2575-2580, 10.1073/pnas.1212089110, 2013.
- 1101 Despres, V. R., Nowoisky, J. F., Klose, M., Conrad, R., Andreae, M. O., and Pöschl, U.:  
1102 Characterization of primary biogenic aerosol particles in urban, rural, and high-alpine air by  
1103 DNA sequence and restriction fragment analysis of ribosomal RNA genes, Biogeosciences, 4,  
1104 1127-1141, 2007.
- 1105 Despres, V. R., Huffman, J. A., Burrows, S. M., Hoose, C., Safatov, A. S., Buryak, G., Frohlich-  
1106 Nowoisky, J., Elbert, W., Andreae, M. O., Pöschl, U., and Jaenicke, R.: Primary biological  
1107 aerosol particles in the atmosphere: a review, Tellus Series B-Chemical and Physical  
1108 Meteorology, 64, 10.3402/tellusb.v64i0.15598, 2012.
- 1109 Du, C., Liu, S., Yu, X., Li, X., Chen, C., Peng, Y., Dong, Y., Dong, Z., and Wang, F.: Urban  
1110 Boundary Layer Height Characteristics and Relationship with Particulate Matter Mass  
1111 Concentrations in Xi'an, Central China, Aerosol and Air Quality Research, 13, 1598-1607,  
1112 10.4209/aaqr.2012.10.0274, 2013.
- 1113 Elbert, W., Taylor, P. E., Andreae, M. O., and Pöschl, U.: Contribution of fungi to primary  
1114 biogenic aerosols in the atmosphere: wet and dry discharged spores, carbohydrates, and  
1115 inorganic ions, Atmospheric Chemistry and Physics, 7, 4569-4588, 2007.
- 1116 Emberlin, J., Newman, T., and Bryant, R.: The incidence of fungal spores in the ambient air and  
1117 inside homes: Evidence from London, Aerobiologia, 11, 253-258, 10.1007/bf02447205, 1995
- 1118 Fisher, M. C., Henk, D. A., Briggs, C. J., Brownstein, J. S., Madoff, L. C., McCraw, S. L., and  
1119 Gurr, S. J.: Emerging fungal threats to animal, plant and ecosystem health, Nature, 484, 186-194,  
1120 10.1038/nature10947, 2012.
- 1121 Fröhlich-Nowoisky, J., Pickersgill, D. A., Després, V. R., and Pöschl, U.: High diversity of fungi  
1122 in air particulate matter, Proceedings of the National Academy of Sciences, 106, 12814-12819,  
1123 10.1073/pnas.0811003106, 2009.
- 1124 Froehlich-Nowoisky, J., Burrows, S. M., Xie, Z., Engling, G., Solomon, P. A., Fraser, M. P.,  
1125 Mayol-Bracero, O. L., Artaxo, P., Begerow, D., Conrad, R., Andreae, M. O., Despres, V. R., and





- 1126 Poeschl, U.: Biogeography in the air: fungal diversity over land and oceans, *Biogeosciences*, 9,  
1127 1125-1136, 10.5194/bg-9-1125-2012, 2012.
- 1128 Fuzzi, S., Mandrioli, P., and Peretto, A.: Fog droplets - An atmospheric source of secondary  
1129 biological aerosol particles, *Atmospheric Environment*, 31, 287-290, 10.1016/1352-  
1130 2310(96)00160-4, 1997.
- 1131 Gabey, A. M., Gallagher, M. W., Whitehead, J., Dorsey, J. R., Kaye, P. H., and Stanley, W. R.:  
1132 Measurements and comparison of primary biological aerosol above and below a tropical forest  
1133 canopy using a dual channel fluorescence spectrometer, *Atmospheric Chemistry and Physics*, 10,  
1134 4453-4466, 10.5194/acp-10-4453-2010, 2010.
- 1135 Gabey, A. M., Stanley, W. R., Gallagher, M. W., and Kaye, P. H.: The fluorescence properties of  
1136 aerosol larger than 0.8  $\mu\text{m}$  in urban and tropical rainforest locations, *Atmospheric Chemistry  
1137 and Physics*, 11, 5491-5504, 10.5194/acp-11-5491-2011, 2011.
- 1138 Gabey, A. M., Vaitilingom, M., Freney, E., Boulon, J., Sellegri, K., Gallagher, M. W., Crawford,  
1139 I. P., Robinson, N. H., Stanley, W. R., and Kaye, P. H.: Observations of fluorescent and  
1140 biological aerosol at a high-altitude site in central France, *Atmospheric Chemistry and Physics*,  
1141 13, 7415-7428, 10.5194/acp-13-7415-2013, 2013.
- 1142 Gangamma, S.: Characteristics of airborne bacteria in Mumbai urban environment, *Science of  
1143 the Total Environment*, 488, 70-74, 10.1016/j.scitotenv.2014.04.065, 2014.
- 1144 Garland, R. M., Schmid, O., Nowak, A., Achtert, P., Wiedensohler, A., Gunthe, S. S., Takegawa,  
1145 N., Kita, K., Kondo, Y., Hu, M., Shao, M., Zeng, L. M., Zhu, T., Andreae, M. O., and Pöschl, U.:  
1146 Aerosol optical properties observed during Campaign of Air Quality Research in Beijing 2006  
1147 (CAREBeijing-2006): Characteristic differences between the inflow and outflow of Beijing city  
1148 air, *Journal of Geophysical Research-Atmospheres*, 114, 2009.
- 1149 Grand, L. F., and Vandyke, C. G.: Scanning electron microscopy of basidiospores of species of  
1150 *hydnum*, *hydnum*, *phellodon*, and *bankera* (*hydnum*), *Journal of the Elisha Mitchell  
1151 Scientific Society*, 92, 114-123, 1976.
- 1152 Hairston, P. P., Ho, J., and Quant, F. R.: Design of an instrument for real-time detection of  
1153 bioaerosols using simultaneous measurement of particle aerodynamic size and intrinsic  
1154 fluorescence, *Journal of Aerosol Science*, 28, 471-482, 10.1016/s0021-8502(96)00448-x, 1997.
- 1155 Hallar, A. G., Chirokova, G., McCubbin, I., Painter, T. H., Wiedinmyer, C., and Dodson, C.:  
1156 Atmospheric bioaerosols transported via dust storms in the western United States, *Geophysical  
1157 Research Letters*, 38, 10.1029/2011gl048166, 2011.
- 1158 Hameed, A. A. A., Khoder, M. I., Ibrahim, Y. H., Saeed, Y., Osman, M. E., and Ghanem, S.:  
1159 Study on some factors affecting survivability of airborne fungi, *Science of the Total  
1160 Environment*, 414, 696-700, 10.1016/j.scitotenv.2011.10.042, 2012.



- 1161 Hameed, A. A. A., Khoder, M. I., Yuosra, S., Osman, A. M., and Ghanem, S.: Diurnal  
1162 distribution of airborne bacteria and fungi in the atmosphere of Helwan area, Egypt, *Science of*  
1163 *the Total Environment*, 407, 6217-6222, 10.1016/j.scitotenv.2009.08.028, 2009.
- 1164 Hara, K., and Zhang, D.: Bacterial abundance and viability in long-range transported dust,  
1165 *Atmospheric Environment*, 47, 20-25, 10.1016/j.atmosenv.2011.11.050, 2012.
- 1166 Hasnain, S. M.: Influence of meteorological factors on the air spora, *Grana*, 32, 184-188, 1993.
- 1167 Healy, D. A., Huffman, J. A., O'Connor, D. J., Poehlker, C., Poeschl, U., and Sodeau, J. R.:  
1168 Ambient measurements of biological aerosol particles near Killarney, Ireland: a comparison  
1169 between real-time fluorescence and microscopy techniques, *Atmospheric Chemistry and Physics*,  
1170 14, 8055-8069, 10.5194/acp-14-8055-2014, 2014.
- 1171 Herrero, B., FombellaBlanco, M. A., FernandezGonzalez, D., and ValenciaBarrera, R. M.: The  
1172 role of meteorological factors in determining the annual variation of *Alternaria* and  
1173 *Cladosporium* spores in the atmosphere of Palencia, 1990-1992, *International Journal of*  
1174 *Biometeorology*, 39, 139-142, 10.1007/bf01211226, 1996.
- 1175 Hirst, J. M.: Changes in atmospheric spore content: Diurnal periodicity and the effects of  
1176 weather, *Transactions of the British Mycological Society*, 36, 375-IN378,  
1177 [http://dx.doi.org/10.1016/S0007-1536\(53\)80034-3](http://dx.doi.org/10.1016/S0007-1536(53)80034-3), 1953.
- 1178 Hjelmroos, M.: Relationship between airborne fungal spore presence and weather variables -  
1179 *cladosporium and alternaria*, *Grana*, 32, 40-47, 1993.
- 1180 Ho, H. M., Rao, C. Y., Hsu, H. H., Chiu, Y. H., Liu, C. M., and Chao, H. J.: Characteristics and  
1181 determinants of ambient fungal spores in Hualien, Taiwan, *Atmospheric Environment*, 39, 5839-  
1182 5850, 10.1016/j.atmosenv.2005.06.034, 2005.
- 1183 Hollins, P. D., Kettlewell, P. S., Atkinson, M. D., Stephenson, D. B., Corden, J. M., Millington,  
1184 W. M., and Mullins, J.: Relationships between airborne fungal spore concentration of  
1185 *Cladosporium* and the summer climate at two sites in Britain, *International Journal of*  
1186 *Biometeorology*, 48, 137-141, 10.1007/s00484-003-0188-9, 2004.
- 1187 Horner, W. E., Oneil, C. E., and Lehrer, S. B.: Basidiospore aeroallergens, *Clinical Reviews in*  
1188 *Allergy*, 10, 191-211, 1992.
- 1189 Huffman, J. A., Treutlein, B., and Pöschl, U.: Fluorescent biological aerosol particle  
1190 concentrations and size distributions measured with an Ultraviolet Aerodynamic Particle Sizer  
1191 (UV-APS) in Central Europe, *Atmos. Chem. Phys.*, 10, 3215-3233, 2010.
- 1192 Huffman, J. A., Sinha, B., Garland, R. M., Snee-Pollmann, A., Gunthe, S. S., Artaxo, P., Martin,  
1193 S. T., Andreae, M. O., and Pöschl, U.: Size distributions and temporal variations of biological  
1194 aerosol particles in the Amazon rainforest characterized by microscopy and real-time UV-APS  
1195 fluorescence techniques during AMAZE-08, *Atmospheric Chemistry and Physics*, 12, 11997-  
1196 12019, 10.5194/acp-12-11997-2012, 2012.



- 1197 Huffman, J. A., Prenni, A. J., DeMott, P. J., Poehlker, C., Mason, R. H., Robinson, N. H.,  
1198 Froehlich-Nowoisky, J., Tobo, Y., Despres, V. R., Garcia, E., Gochis, D. J., Harris, E., Mueller-  
1199 Germann, I., Ruzene, C., Schmer, B., Sinha, B., Day, D. A., Andreae, M. O., Jimenez, J. L.,  
1200 Gallagher, M., Kreidenweis, S. M., Bertram, A. K., and Poeschl, U.: High concentrations of  
1201 biological aerosol particles and ice nuclei during and after rain, *Atmospheric Chemistry and*  
1202 *Physics*, 13, 6151-6164, 10.5194/acp-13-6151-2013, 2013.
- 1203 Jones, A. M., and Harrison, R. M.: The effects of meteorological factors on atmospheric  
1204 bioaerosol concentrations - a review, *Science of the Total Environment*, 326, 151-180,  
1205 10.1016/j.scitotenv.2003.11.021, 2004.
- 1206 Kanaani, H., Hargreaves, M., Ristovski, Z., and Morawska, L.: Performance assessment of  
1207 UVAPS: Influence of fungal spore age and air exposure, *Journal of Aerosol Science*, 38, 83-96,  
1208 10.1016/j.jaerosci.2006.10.003, 2007.
- 1209 Kanaani, H., Hargreaves, M., Smith, J., Ristovski, Z., Agranovski, V., and Morawska, L.:  
1210 Performance of UVAPS with respect to detection of airborne fungi, *Journal of Aerosol Science*,  
1211 39, 175-189, 10.1016/j.jaerosci.2007.10.007, 2008.
- 1212 Kanawade, V. P., Shika, S., Poehlker, C., Rose, D., Suman, M. N. S., Gadhavi, H., Kumar, A.,  
1213 Nagendra, S. M. S., Ravikrishna, R., Yu, H., Sahu, L. K., Jayaraman, A., Andreae, M. O.,  
1214 Poeschl, U., and Gunthe, S. S.: Infrequent occurrence of new particle formation at a semi-rural  
1215 location, Gadanki, in tropical Southern India, *Atmospheric Environment*, 94, 264-273,  
1216 10.1016/j.atmosenv.2014.05.046, 2014.
- 1217 Kurkela, T.: The number of *Cladosporium* conidia in the air in different weather conditions,  
1218 *Grana*, 36, 54-61, 1997.
- 1219 Lee, S.-H., Lee, H.-J., Kim, S.-J., Lee, H. M., Kang, H., and Kim, Y. P.: Identification of  
1220 airborne bacterial and fungal community structures in an urban area by T-RFLP analysis and  
1221 quantitative real-time PCR, *Science of the Total Environment*, 408, 1349-1357,  
1222 10.1016/j.scitotenv.2009.10.061, 2010.
- 1223 Levetin, E., and Horner, W. E.: Fungal aerobiology: Exposure and measurement, *Fungal Allergy*  
1224 *and Pathogenicity*, 81, 10-27, 2002.
- 1225 Li, D. W., and Kendrick, B.: Functional-relationships between airborne fungal spores and  
1226 environmental-factors in Kitchener-Waterloo, Ontario, as detected by canonical correspondence-  
1227 analysis, *Grana*, 33, 166-176, 1994.
- 1228 Li, F., and Ramanathan, V.: Winter to summer monsoon variation of aerosol optical depth over  
1229 the tropical Indian Ocean, *Journal of Geophysical Research-Atmospheres*, 107,  
1230 10.1029/2001jd000949, 2002.
- 1231 Li, M., Qi, J., Zhang, H., Huang, S., Li, L., and Gao, D.: Concentration and size distribution of  
1232 bioaerosols in an outdoor environment in the Qingdao coastal region, *Science of the Total*  
1233 *Environment*, 409, 3812-3819, 10.1016/j.scitotenv.2011.06.001, 2011.



- 1234 Lyon, F. L., Kramer, C. L., and Eversmeyer, M. G.: Variation of airspora in the atmosphere due  
1235 to weather conditions, Grana, 23, 177-181, 1984.
- 1236 Madden, L. V.: Effects of rain on splash dispersal of fungal pathogens, Canadian Journal of Plant  
1237 Pathology, 19, 225-230, 1997.
- 1238 Maki, T., Kakikawa, M., Kobayashi, F., Yamada, M., Matsuki, A., Hasegawa, H., and Iwasaka,  
1239 Y.: Assessment of composition and origin of airborne bacteria in the free troposphere over Japan,  
1240 Atmospheric Environment, 74, 73-82, 10.1016/j.atmosenv.2013.03.029, 2013.
- 1241 Matthias-Maser, S., Obolkin, V., Khodzer, T., and Jaenicke, R.: Seasonal variation of primary  
1242 biological aerosol particles in the remote continental region of Lake Baikal/Siberia, Atmospheric  
1243 Environment, 34, 3805-3811, 10.1016/s1352-2310(00)00139-4, 2000.
- 1244 Matthiasmaser, S., and Jaenicke, R.: A method to identify biological aerosol-particles with radius  
1245 greater-than 0.3  $\mu\text{m}$  for the determination of their size distribution, Journal of Aerosol Science,  
1246 22, S849-S852, 10.1016/s0021-8502(05)80232-0, 1991.
- 1247 Matthiasmaser, S., and Jaenicke, R.: Examination of atmospheric bioaerosol particles with radii  
1248 greater-than-0.2  $\mu\text{m}$ , Journal of Aerosol Science, 25, 1605-1613, 10.1016/0021-8502(94)90228-  
1249 3, 1994.
- 1250 MatthiasMaser, S., and Jaenicke, R.: The size distribution of primary biological aerosol particles  
1251 with radii  $>0.2 \mu\text{m}$  in an urban rural influenced region, Atmospheric Research, 39, 279-286,  
1252 10.1016/0169-8095(95)00017-8, 1995.
- 1253 Moehler, O., DeMott, P. J., Vali, G., and Levin, Z.: Microbiology and atmospheric processes: the  
1254 role of biological particles in cloud physics, Biogeosciences, 4, 1059-1071, 2007.
- 1255 Moorthy, K. K., Nair, P. R., and Murthy, B. V. K.: Size distribution of coastal aerosols - effects  
1256 of local-sources and sinks, Journal of Applied Meteorology, 30, 844-852, 10.1175/1520-  
1257 0450(1991)030<0844:sdocae>2.0.co;2, 1991.
- 1258 Morris, C. E., Georgakopoulos, D. G., and Sands, D. C.: Ice nucleation active bacteria and their  
1259 potential role in precipitation, Journal De Physique Iv, 121, 87-103, 10.1051/jp4:2004121004,  
1260 2004.
- 1261 Morris, C. E., Conen, F., Huffman, J. A., Phillips, V., Poeschl, U., and Sands, D. C.:  
1262 Bioprecipitation: a feedback cycle linking Earth history, ecosystem dynamics and land use  
1263 through biological ice nucleators in the atmosphere, Global Change Biology, 20, 341-351,  
1264 10.1111/gcb.12447, 2014.
- 1265 Myers, N., Mittermeier, R. A., Mittermeier, C. G., da Fonseca, G. A. B., and Kent, J.:  
1266 Biodiversity hotspots for conservation priorities, Nature, 403, 853-858, 10.1038/35002501, 2000.
- 1267 Naja, M., and Lal, S.: Surface ozone and precursor gases at Gadanki (13.5 degrees N, 79.2  
1268 degrees E), a tropical rural site in India, Journal of Geophysical Research-Atmospheres, 107,  
1269 10.1029/2001jd000357, 2002.



- 1270 Oh, J.-W., Lee, H.-B., Lee, H.-R., Pyun, B.-Y., Ahn, Y.-M., Kim, K.-E., Lee, S.-Y., and Lee, S.-  
1271 I.: Aerobiological study of pollen and mold in Seoul, Korea, *Allergology International*, 47, 263-  
1272 270, <http://dx.doi.org/10.2332/allergolint.47.263>, 1998.
- 1273 Oliveira, M., Amorim, M. I., Ferreira, E., Delgado, L., and Abreu, I.: Main airborne Ascomycota  
1274 spores: characterization by culture, spore morphology, ribosomal DNA sequences and enzymatic  
1275 analysis, *Applied Microbiology and Biotechnology*, 86, 1171-1181, 10.1007/s00253-010-2448-z,  
1276 2010.
- 1277 Pachauri, T., Singla, V., Satsangi, A., Lakhani, A., and Kumari, K. M.: Characterization of major  
1278 pollution events (dust, haze, and two festival events) at Agra, India, *Environmental Science and*  
1279 *Pollution Research*, 20, 5737-5752, 10.1007/s11356-013-1584-2, 2013.
- 1280 Pan, Y. L., Holler, S., Chang, R. K., Hill, S. C., Pinnick, R. G., Niles, S., and Bottiger, J. R.:  
1281 Single-shot fluorescence spectra of individual micrometer-sized bioaerosols illuminated by a  
1282 351- or a 266-nm ultraviolet laser, *Optics Letters*, 24, 116-118, 10.1364/ol.24.000116, 1999a.
- 1283 Pan, Y. L., Holler, S., Chang, R. K., Hill, S. C., Pinnick, R. G., Niles, S., Bottiger, J. R., and  
1284 Bronk, B. V.: Real-time detection and characterization of individual flowing airborne biological  
1285 particles: fluorescence spectra and elastic scattering measurements, in: *Air Monitoring and*  
1286 *Detection of Chemical and Biological Agents II*, edited by: Leonelli, J., and Althouse, M. L.,  
1287 *Proceedings of the Society of Photo-Optical Instrumentation Engineers (Spie)*, 117-125, 1999b.
- 1288 Poehlker, C., Huffman, J. A., and Poeschl, U.: Autofluorescence of atmospheric bioaerosols -  
1289 fluorescent biomolecules and potential interferences, *Atmospheric Measurement Techniques*, 5,  
1290 37-71, 10.5194/amt-5-37-2012, 2012.
- 1291 Poehlker, C., Huffman, J. A., Foerster, J. D., and Poeschl, U.: Autofluorescence of atmospheric  
1292 bioaerosols: spectral fingerprints and taxonomic trends of pollen, *Atmospheric Measurement*  
1293 *Techniques*, 6, 3369-3392, 10.5194/amt-6-3369-2013, 2013.
- 1294 Pöschl, U.: Atmospheric aerosols: Composition, transformation, climate and health effects,  
1295 *Angewandte Chemie-International Edition*, 44, 7520-7540, 10.1002/anie.200501122, 2005.
- 1296 Pöschl, U., Martin, S. T., Sinha, B., Chen, Q., Gunthe, S. S., Huffman, J. A., Borrmann, S.,  
1297 Farmer, D. K., Garland, R. M., Helas, G., Jimenez, J. L., King, S. M., Manzi, A., Mikhailov, E.,  
1298 Pauliquevis, T., Petters, M. D., Prenni, A. J., Roldin, P., Rose, D., Schneider, J., Su, H., Zorn, S.  
1299 R., Artaxo, P., and Andreae, M. O.: Rainforest Aerosols as Biogenic Nuclei of Clouds and  
1300 Precipitation in the Amazon, *Science*, 329, 1513-1516, 10.1126/science.1191056, 2010.
- 1301 Pranesha, T. S., and Kamra, A. K.: Scavenging of aerosol particles by large water drops .2. The  
1302 effect of electrical forces, *Journal of Geophysical Research-Atmospheres*, 102, 23937-23946,  
1303 10.1029/97jd01834, 1997a.
- 1304 Pranesha, T. S., and Kamra, A. K.: Scavenging of aerosol particles by large water drops .3.  
1305 Washout coefficients, half-lives, and rainfall depths, *Journal of Geophysical Research-*  
1306 *Atmospheres*, 102, 23947-23953, 10.1029/97jd01835, 1997b.



- 1307 Prenni, A. J., Petters, M. D., Kreidenweis, S. M., Heald, C. L., Martin, S. T., Artaxo, P., Garland,  
1308 R. M., Wollny, A. G., and Poschl, U.: Relative roles of biogenic emissions and Saharan dust as  
1309 ice nuclei in the Amazon basin, *Nature Geoscience*, 2, 401-404, 2009.
- 1310 Prenni, A. J., Tobo, Y., Garcia, E., DeMott, P. J., Huffman, J. A., McCluskey, C. S.,  
1311 Kreidenweis, S. M., Prenni, J. E., Poehlker, C., and Poeschl, U.: The impact of rain on ice nuclei  
1312 populations at a forested site in Colorado, *Geophysical Research Letters*, 40, 227-231,  
1313 10.1029/2012gl053953, 2013.
- 1314 Prospero, J. M.: Mineral and sea salt aerosol concentrations in various ocean regions, *Journal of*  
1315 *Geophysical Research-Oceans and Atmospheres*, 84, 725-731, 10.1029/JC084iC02p00725,  
1316 1979.
- 1317 Prospero, J. M., Blades, E., Mathison, G., and Naidu, R.: Interhemispheric transport of viable  
1318 fungi and bacteria from Africa to the Caribbean with soil dust, *Aerobiologia*, 21, 1-19,  
1319 10.1007/s10453-004-5872-7, 2005.
- 1320 Quintero, E., Rivera-Mariani, F., and Bolanos-Rosero, B.: Analysis of environmental factors and  
1321 their effects on fungal spores in the atmosphere of a tropical urban area (San Juan, Puerto Rico),  
1322 *Aerobiologia*, 26, 113-124, 10.1007/s10453-009-9148-0, 2010.
- 1323 Raatikainen, T., Hyvarinen, A. P., Hatakka, J., Panwar, T. S., Hooda, R. K., Sharma, V. P., and  
1324 Lihavainen, H.: The effect of boundary layer dynamics on aerosol properties at the Indo-  
1325 Gangetic plains and at the foothills of the Himalayas, *Atmospheric Environment*, 89, 548-555,  
1326 10.1016/j.atmosenv.2014.02.058, 2014.
- 1327 Radke, L. F., Hobbs, P. V., and Eltgroth, M. W.: Scavenging of aerosol-particles by  
1328 precipitation, *Journal of Applied Meteorology*, 19, 715-722, 10.1175/1520-  
1329 0450(1980)019<0715:soapbp>2.0.co;2, 1980.
- 1330 Saari, S., Niemi, J. V., Ronkko, T., Kuuluvainen, H., Jarvinen, A., Pirjola, L., Aurela, M.,  
1331 Hillamo, R., and Keskinen, J.: Seasonal and Diurnal Variations of Fluorescent Bioaerosol  
1332 Concentration and Size Distribution in the Urban Environment, *Aerosol and Air Quality*  
1333 *Research*, 15, 572-581, 10.4209/aaqr.2014.10.0258, 2015.
- 1334 Sabariego, S., de la Guardia, C. D., and Alba, F.: The effect of meteorological factors on the  
1335 daily variation of airborne fungal spores in Granada (southern Spain), *International Journal of*  
1336 *Biometeorology*, 44, 1-5, 10.1007/s004840050131, 2000.
- 1337 Sady, M., Skjoth, C. A., and Kennedy, R.: Back-trajectories show export of airborne fungal  
1338 spores (*Ganoderma* sp.) from forests to agricultural and urban areas in England, *Atmospheric*  
1339 *Environment*, 84, 88-99, 10.1016/j.atmosenv.2013.11.015, 2014.
- 1340 Santarpia, J. L., Ratnesar-Shumate, S., Gilberry, J. U., and Quizon, J. J.: Relationship Between  
1341 Biologically Fluorescent Aerosol and Local Meteorological Conditions, *Aerosol Sci. Technol.*,  
1342 47, 655-661, 10.1080/02786826.2013.781263, 2013.





- 1343 Satheesh, S. K., and Srinivasan, J.: Enhanced aerosol loading over Arabian Sea during the pre-  
1344 monsoon season: Natural or anthropogenic?, *Geophysical Research Letters*, 29,  
1345 10.1029/2002gl015687, 2002.
- 1346 Schumacher, C. J., Poehlker, C., Aalto, P., Hiltunen, V., Petaja, T., Kulmala, M., Poeschl, U.,  
1347 and Huffman, J. A.: Seasonal cycles of fluorescent biological aerosol particles in boreal and  
1348 semi-arid forests of Finland and Colorado, *Atmospheric Chemistry and Physics*, 13, 11987-  
1349 12001, 10.5194/acp-13-11987-2013, 2013.
- 1350 Sesartic, A., and Dallafior, T. N.: Global fungal spore emissions, review and synthesis of  
1351 literature data, *Biogeosciences*, 8, 1181-1192, 10.5194/bg-8-1181-2011, 2011.
- 1352 Shaffer, B. T., and Lighthart, B.: Survey of culturable airborne bacteria at four diverse locations  
1353 in Oregon: Urban, rural, forest, and coastal, *Microbial Ecology*, 34, 167-177,  
1354 10.1007/s002489900046, 1997.
- 1355 Sharma, N. K., and Rai, A. K.: Allergenicity of airborne cyanobacteria *Phormidium fragile* and  
1356 *Nostoc muscorum*, *Ecotoxicology and Environmental Safety*, 69, 158-162,  
1357 10.1016/j.ecoenv.2006.08.006, 2008.
- 1358 Sherman, J. P., Sheridan, P. J., Ogren, J. A., Andrews, E., Hageman, D., Schmeisser, L.,  
1359 Jefferson, A., and Sharma, S.: A multi-year study of lower tropospheric aerosol variability and  
1360 systematic relationships from four North American regions, *Atmospheric Chemistry and Physics*,  
1361 15, 12487-12517, 10.5194/acp-15-12487-2015, 2015.
- 1362 Shika, S., et al.: Atmospheric aerosol properties at a semi-rural location in South India: particle  
1363 size distributions and implications for cloud formation, to be submitted.
- 1364 Sivaprakasam, V., Huston, A. L., Scotto, C., and Eversole, J. D.: Multiple UV wavelength  
1365 excitation and fluorescence of bioaerosols, *Optics Express*, 12, 4457-4466,  
1366 10.1364/opex.12.004457, 2004.
- 1367 Spracklen, D. V., and Heald, C. L.: The contribution of fungal spores and bacteria to regional  
1368 and global aerosol number and ice nucleation immersion freezing rates, *Atmospheric Chemistry  
1369 and Physics*, 14, 9051-9059, 10.5194/acp-14-9051-2014, 2014.
- 1370 Srivastava, A., Singh, M., and Jain, V. K.: Identification and characterization of size-segregated  
1371 bioaerosols at Jawaharlal Nehru University, New Delhi, *Natural Hazards*, 60, 485-499,  
1372 10.1007/s11069-011-0022-3, 2012.
- 1373 Tarlo, S. M., Bell, B., Srinivasan, J., Dolovich, J., and Hargreave, F. E.: Human sensitization to  
1374 ganoderma antigen, *Journal of Allergy and Clinical Immunology*, 64, 43-49, 10.1016/0091-  
1375 6749(79)90082-4, 1979.
- 1376 Tong, Y and Lighthart, B.: Diurnal Distribution of Total and Culturable Atmospheric Bacteria at  
1377 a Rural Site, *Aerosol Sci. Technol.*, 30, 246-254, 10.1080/027868299304822, 1999.



- 1378 Toprak, E., and Schnaiter, M.: Fluorescent biological aerosol particles measured with the  
1379 Waveband Integrated Bioaerosol Sensor WIBS-4: laboratory tests combined with a one year  
1380 field study, *Atmospheric Chemistry and Physics*, 13, 225-243, 10.5194/acp-13-225-2013, 2013.
- 1381 Trejo, M., Douarche, C., Bailleux, V., Poulard, C., Mariot, S., Regeard, C., and Raspaud, E.:  
1382 Elasticity and wrinkled morphology of *Bacillus subtilis* pellicles, *Proceedings of the National*  
1383 *Academy of Sciences of the United States of America*, 110, 2011-2016,  
1384 10.1073/pnas.1217178110, 2013.
- 1385 Troutt, C., and Levetin, E.: Correlation of spring spore concentrations and meteorological  
1386 conditions in Tulsa, Oklahoma, *International Journal of Biometeorology*, 45, 64-74,  
1387 10.1007/s004840100087, 2001.
- 1388 Valsan, A. E., Priyamvada, H., Ravikrishna, R., Després, V. R., Biju, C. V., Sahu, L. K., Kumar,  
1389 A., Verma, R. S., Philip, L., and Gunthe, S. S.: Morphological characteristics of bioaerosols from  
1390 contrasting locations in southern tropical India – A case study, *Atmospheric Environment*, 122,  
1391 321-331, <http://dx.doi.org/10.1016/j.atmosenv.2015.09.071>, 2015.
- 1392 Vinoj, V., and Satheesh, S. K.: Measurements of aerosol optical depth over Arabian Sea during  
1393 summer monsoon season, *Geophysical Research Letters*, 30, 10.1029/2002gl016664, 2003.
- 1394 Vinoj, V., Satheesh, S. K., and Moorthy, K. K.: Optical, radiative, and source characteristics of  
1395 aerosols at Minicoy, a remote island in the southern Arabian Sea, *Journal of Geophysical*  
1396 *Research-Atmospheres*, 115, 10.1029/2009jd011810, 2010.
- 1397 Vinoj, V., Rasch, P. J., Wang, H., Yoon, J.-H., Ma, P.-L., Landu, K., and Singh, B.: Short-term  
1398 modulation of Indian summer monsoon rainfall by West Asian dust, *Nature Geoscience*, 7, 308-  
1399 313, 10.1038/ngeo2107, 2014.
- 1400 Wang, C.-C., Fang, G.-C., and Lee, L.: Bioaerosols study in central Taiwan during summer  
1401 season, *Toxicology and Industrial Health*, 23, 133-139, 10.1177/0748233707078741, 2007.
- 1402 Yu, X., Wang, Z., Zhang, M., Kuhn, U., Xie, Z., Cheng, Y., Pöschl, U., and Su, H.: Ambient  
1403 measurement of fluorescent aerosol particles with a WIBS in the Yangtze River Delta of China:  
1404 potential impacts of combustion-generated aerosol particles, *Atmos. Chem. Phys. Discuss.*,  
1405 doi:10.5194/acp-2016-228, in review, 2016.
- 1406 Zhang, T., Engling, G., Chan, C.-Y., Zhang, Y.-N., Zhang, Z.-S., Lin, M., Sang, X.-F., Li, Y. D.,  
1407 and Li, Y.-S.: Contribution of fungal spores to particulate matter in a tropical rainforest,  
1408 *Environmental Research Letters*, 5, 10.1088/1748-9326/5/2/024010, 2010.
- 1409
- 1410





1411 Table 1: List of frequently used acronyms and symbols with units.

1412

1413

Symbol	Quantity, Unit	
$D_a$	Aerodynamic diameter, $\mu\text{m}$	1414
$D_g$	Geometric midpoint diameter of fluorescent particles	1415
$D_{g,T}$	Geometric midpoint diameter of total particles	1416
DNA	Deoxyribonucleic acid	
FBAP	Fluorescent biological aerosol particle	1417
He-Ne	Helium-Neon	1418
ITCZ	Inter Tropical Convergence Zone	
$M_F$	Integrated mass concentration of fluorescent particles, $\mu\text{g m}^{-3}$	1419
$M_T$	Integrated mass concentration of total particles, $\mu\text{g m}^{-3}$	1420
Nd:YAG	Neodymium-doped yttrium Aluminum garnet	
NE	Northeast	1421
$N_F$	Integrated number concentration of fluorescent particles, $\text{cm}^{-3}$	1422
$N_T$	Integrated number concentration of total particles, $\text{cm}^{-3}$	1423
PAH	Polycyclic aromatic hydrocarbon	
PBAPs	Primary Biological Aerosol Particles	1424
RH	Relative Humidity	
SEM	Scanning Electron Microscopy	1425
SW	Southwest	1426
TAP	Total Aerosol Particle	
TSP	Total Suspended Particle	1427
UV-APS	Ultraviolet Aerodynamic Particle Sizer	
$\lambda$	Wavelength, nm	1428

1429

1430

1431

1432

1433

1434

1435

1436



1437

1438

Number		June	July	August	Campaign
$N_T$ (cm <sup>-3</sup> )	Mean	2.66	1.54	0.96	1.77
	Median	2.45	1.48	0.73	1.44
$N_F$ (cm <sup>-3</sup> )	Mean	0.03	0.007	0.015	0.017
	Median	0.02	0.006	0.007	0.01
$N_F/N_T$ (%)	Mean	0.03	0.01	0.03	0.02
	Median	0.01		0.01	0.01
Mass		June	July	August	Campaign
$M_T$ (μg m <sup>-3</sup> )	Mean	10.61	6.15	4.15	7.17
	Median	9.58	5.55	2.8	5.57
$M_F$ (μg m <sup>-3</sup> )	Mean	0.42	0.11	0.18	0.24
	Median	0.33	0.09	0.1	0.15
$M_F/M_T$ (%)	Mean	0.09	0.03	0.08	0.06
	Median	0.04	0.02	0.03	0.03

1439

1440 Table 2: Integrated number concentrations and mass concentrations of coarse TAP and FBAP (~1–20 μm):  
 1441 arithmetic mean and median for each month and for the entire measurement campaign  
 1442

1443

1444

1445

1446

1447

1448

1449

1450

1451



Sl No:	Location	Land Use	Measurement Period	Season	Instrument	FBAP Number Concentration	Total Number Concentration	Number Ratio (%)	Reference
1	Mainz, Central Europe	Semi-urban	Aug-Dec, 2006		UVAPS	$3 \times 10^{-2} \text{ cm}^{-3}$	$1.05 \text{ cm}^{-3}$	4	Huffman et al., 2010
2	Central Amazonia rainforest	Tropical rainforest	Feb-Mar, 2008		UVAPS	$7.3 \times 10^{-2} \text{ cm}^{-3}$	$0.33 \text{ cm}^{-3}$	24	Huffman et al., 2012
3	Manchester, UK	Urban	December, 2009		WIBS-3	$2.9 \times 10^{-4} \text{ cm}^{-3}$ (FL1) $5.2 \times 10^{-4} \text{ cm}^{-3}$ (FL2) $1.1 \times 10^{-5} \text{ cm}^{-3}$ (FL3)	$1.38 \times 10^{-2} \text{ cm}^{-3}$	2.1 3.7 7.8	Gabey et al., 2011
4	Central France	Rural	22 Jun-3 July, 2010		WIBS-3	$1.2 \times 10^{-2} \text{ cm}^{-3}$ (280 nm) $9.5 \times 10^{-2} \text{ cm}^{-3}$ (370 nm)			Gabey et al., 2013
5	Helinski, Finland	Urban	Feb, 2012 (Winter) June-Aug, 2012 (Summer)	Winter Summer	BioScout	$1 \times 10^{-2} \text{ cm}^{-3}$ $2.8 \times 10^{-2} \text{ cm}^{-3}$		23 6	Saari et al., 2015
6	Colarado, USA	Pine forest	June-July, 2011	Summer Dry period Wet Period	UVAPS WIBS-3 WIBS-4	$1.3 \times 10^{-2} \text{ cm}^{-3}$		8 5.8 15.2	Crawford et al., 2014
7	Finland	Rural forest	August, 2009 - April, 2011	Spring Summer Fall Winter	UVAPS	$1.5 \times 10^{-2} \text{ cm}^{-3}$ $4.6 \times 10^{-2} \text{ cm}^{-3}$ $2.7 \times 10^{-2} \text{ cm}^{-3}$ $0.4 \times 10^{-2} \text{ cm}^{-3}$	$0.43 \text{ cm}^{-3}$ $0.45 \text{ cm}^{-3}$ $0.41 \text{ cm}^{-3}$ $0.47 \text{ cm}^{-3}$	4.4 13 9.8 1.1	Schumacher et al., 2013



	Colorado , USA	Rural, semi-arid	2011-2012	Spring	UVAPS	$1.5 \times 10^{-2} \text{ cm}^{-3}$	$0.73 \text{ cm}^{-3}$	2.5	
				Summer		$3 \times 10^{-2} \text{ cm}^{-3}$	$0.44 \text{ cm}^{-3}$	8.8	
				Fall		$1.7 \times 10^{-2} \text{ cm}^{-3}$	$0.28 \text{ cm}^{-3}$	5.7	
				Winter		$0.53 \times 10^{-2} \text{ cm}^{-3}$	$0.2 \text{ cm}^{-3}$	3	
8	Karlsruhe, Germany	Semi-rural	April 2010 - April 2011		WIBS - 4	$3.1 \times 10^{-2} \text{ cm}^{-3}$	$0.583 \text{ cm}^{-3}$	7.34	Toprak and Schnaiter., 2013
9	Nanjing, China	Sub-urban	Oct-Nov, 2013	Autumn	WIBS-4	$0.6 \text{ cm}^{-3}$ (FL1)	$13.1 \text{ cm}^{-3}$	4.6	Yu et al., 2016
						$3.4 \text{ cm}^{-3}$ (FL2)		25.3	
						$2.1 \text{ cm}^{-3}$ (FL3)		15.6	

Table 3: Comparison with other online measurements carried out under various environmental conditions across the globe.



Number		Dusty	Clean	HighBio
$N_T$ (cm <sup>-3</sup> )	Mean	4.2	1.27	1.78
	Median	4.36	1.15	1.4
$N_F$ (cm <sup>-3</sup> )	Mean	0.02	0.005	0.05
	Median	0.019	0.004	0.038
$N_F/N_T$	Mean	0.01	0.01	0.05
	Median			0.03
Mass		Dusty	Clean	HighBio
$M_T$ (μg m <sup>-3</sup> )	Mean	16.34	5.12	7.7
	Median	16.84	4.28	5.85
$M_F$ (μg m <sup>-3</sup> )	Mean	0.36	0.08	0.58
	Median	0.33	0.05	0.47
$M_F/M_T$	Mean	0.02	0.03	0.12
	Median	0.02	0.01	0.08

Table 4: Integrated number concentrations and mass concentrations of coarse TAP and FBAP (~1–20 μm): arithmetic mean and median for each focus period (Dusty, Clean and HighBio).



1470  
 1471  
 1472  
 1473  
 1474  
 1475  
 1476  
 1477  
 1478

	Campaign			Dusty			Clean			High Bio		
	$N_T$	$N_F$	$N_F/N_T$	$N_T$	$N_F$	$N_F/N_T$	$N_T$	$N_F$	$N_F/N_T$	$N_T$	$N_F$	$N_F/N_T$
RH	-0.64	0.58	0.85	-0.25		0.18	-0.66	-0.01	0.13	-0.64	0.5	0.68
Temperature	0.45	-0.65	-0.82	0.34	-0.04	-0.25	0.78	0.02	-0.2	0.43	-0.68	-0.83
Wind Speed	0.4	-0.6	-0.78	0.09	-0.18	-0.31	-0.18	-0.27	0	0.3	-0.61	-0.74

Table 5:  $R^2$  values for correlation between meteorological parameters (RH, Temperature and Wind Speed) and  $N_T$ ,  $N_F$  and  $N_F/N_T$  during the entire campaign and each focus periods.

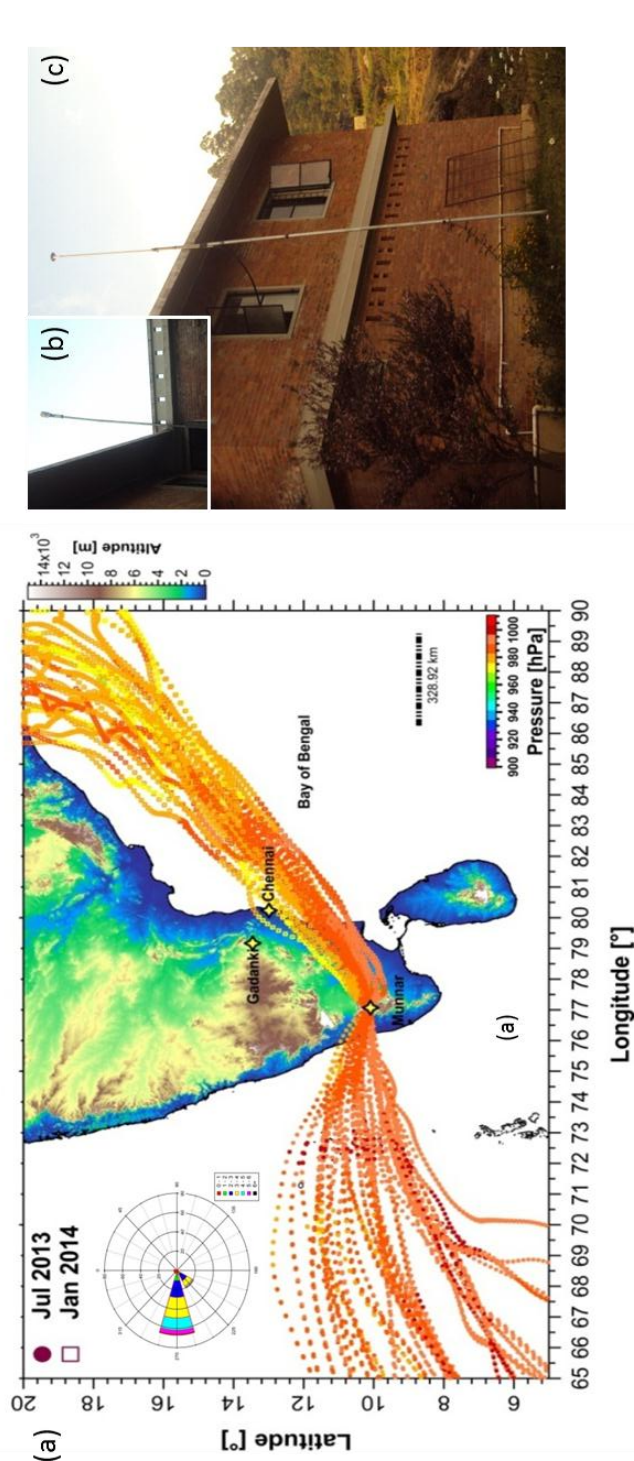


Figure 1: Location of measurement site Mummar (10.09°N, 77.06°E; 1605 m amsl – above mean sea level) located in the Western Ghats mountain range in Southern tropical India with 10 days back trajectories (HYSPLIT, NOAA-ARL GDAS1 model; start height 50 m above ground level; starting time 23:30 local time) illustrating the distinct and contrasting wind patterns during two contrasting seasons; Southwest monsoon season (representative month Jul) and Northeast monsoon season (representative month Jan) when field measurement campaign was carried out. It is evident that predominant wind pattern during Southwest monsoon season was Westerly/Southwesterly bringing the clean marine influx. Also shown in inset is wind rose diagram prepared using the data obtained using the ultrasonic weather station (a). The inlet system prepared for sampling the air using Ultraviolet Aerodynamic Particle Sizer (UV-APS) for bioaerosol number size distribution measurement. Inset shows the arrangement made for installing the ultrasonic weather station (b). The map shown is color-coded by topography (meters).



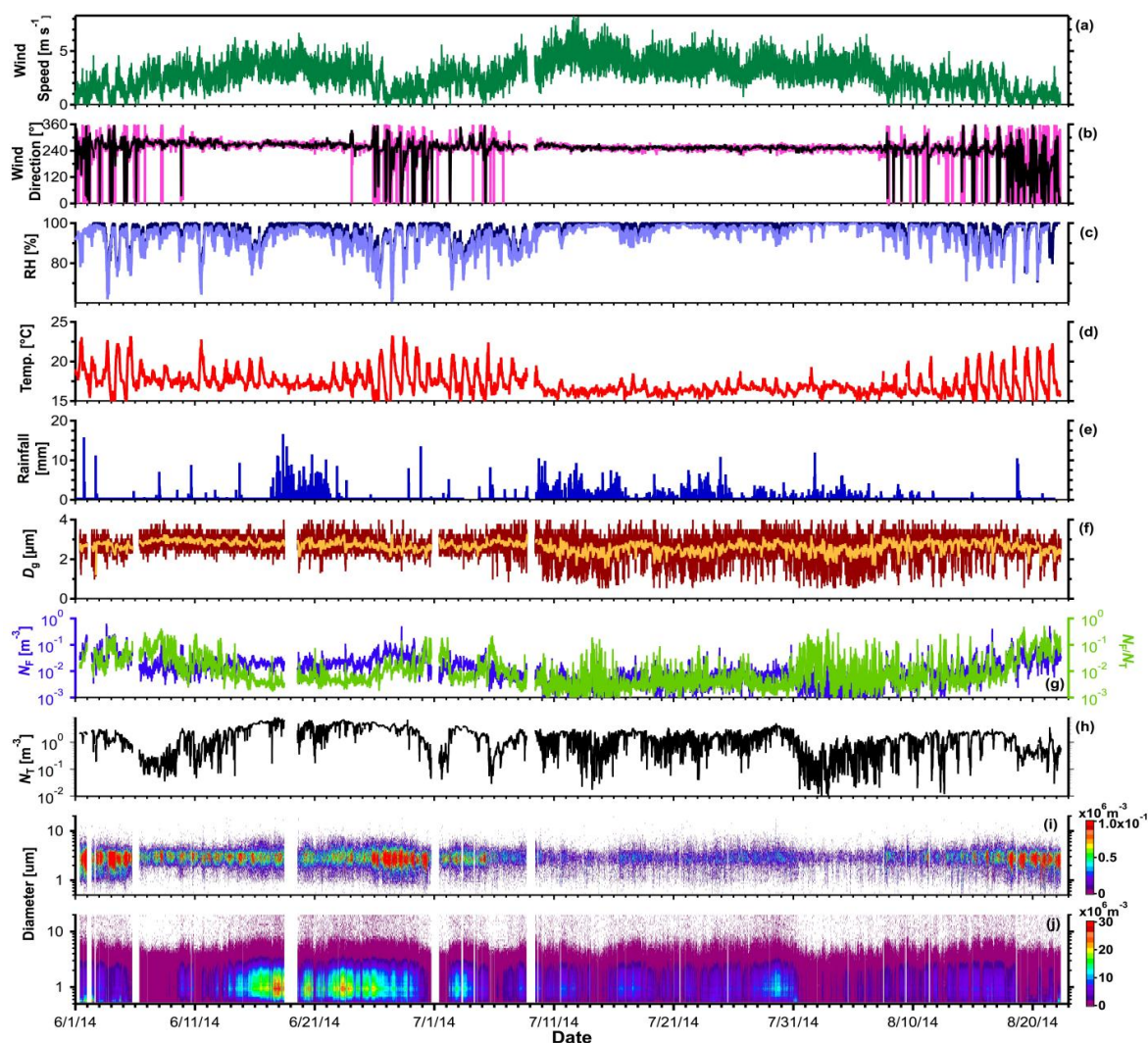


Figure 2: Time series of measured meteorological parameters, parameters derived from FBAP and total particle number size distribution measurements using UV-APS: (a) wind speed, (b) wind direction: five minutes average (magenta) and one hour average (black), (c) relative humidity, (d) temperature, (e) rainfall, (f) geometric mean diameter ( $D_g$ ) five minutes average (dark red) and one hour average (yellow), (g) FBAP number concentration ( $N_F$ ; blue) and relative contribution of FBAP to TAP ( $N_F/N_T$ ; green), (h) TAP number concentration ( $N_T$ ), (i) a contour plot of FBAP number size distribution ( $dN/d\log D_F$ ), and (j) a contour plot of TAP number size distribution ( $dN/d\log D_T$ ). The shadowed block represents the different focus periods (please refer to text for more details).



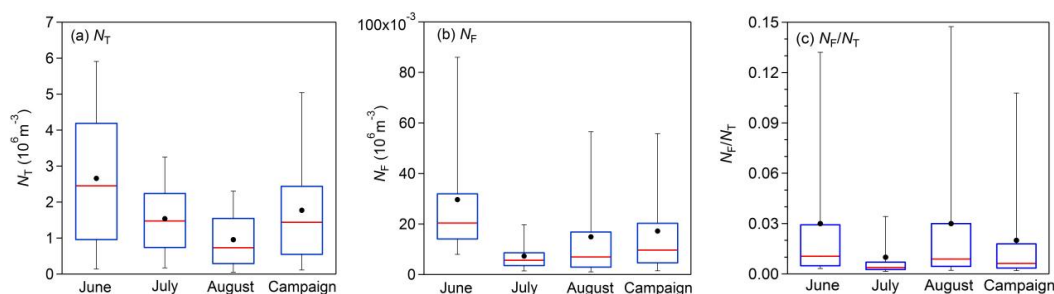


Figure 3: Statistical distribution of integrated ( $\sim 1 - 20 \mu\text{m}$ ) FBAP and TAP number and contribution of  $N_F$  to  $N_T$  measured during each month (Jun – Aug) of SW monsoon season and averaged over the entire measurement campaign carried out at Munnar as box whisker plots: (a) TAP number concentration ( $N_T$ ), (b) FBAP number concentration ( $N_F$ ), and (c) contribution of FBAP number concentration to TAP number concentration ( $N_F/N_T$ ).

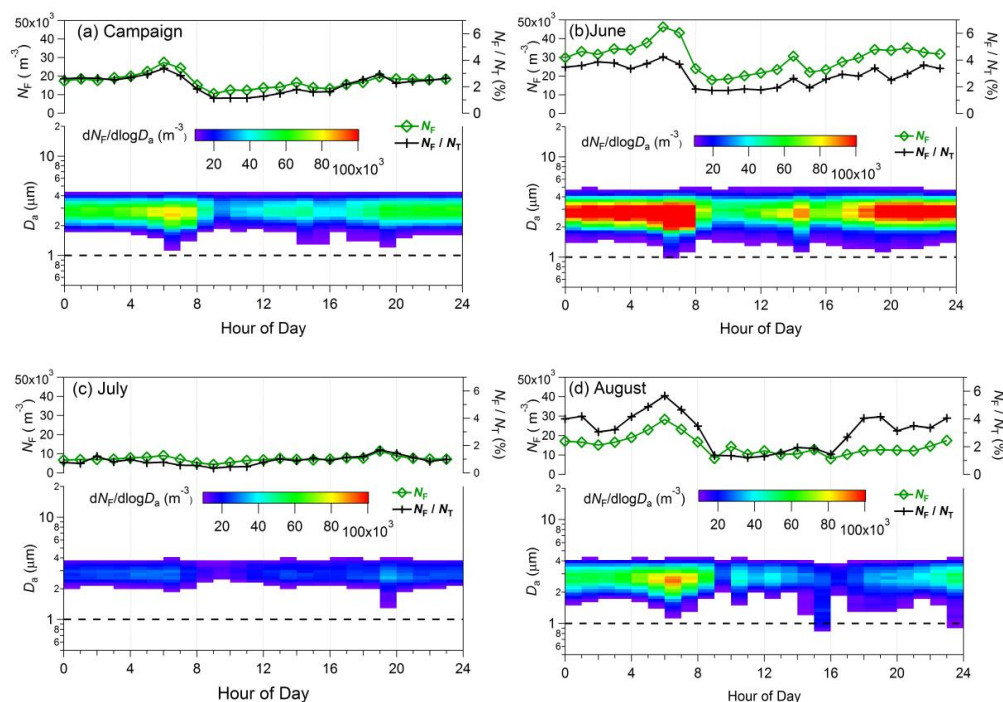


Figure 4: Diurnal cycles of FBAP number concentrations ( $N_F$ ) and size distributions averaged over individual month of measurement and entire campaign (hourly median values plotted against the local time of the day). Upper portion of each panel shows integrated FBAP number concentration ( $\sim 1 - 20 \mu\text{m}$ ;  $N_F$ ) on the left axis (green color) and FBAP fraction of TAP number ( $N_F/N_T$ ) on the right axis (black color). Lower portion of each panel FBAP number size distribution (3-D plot) plotted against hour of the day on x-axis, aerodynamic diameter on y-axis and color is scaled for  $dN_F/d\log D_a$  indicates the concentration. Dashed black lines in lower portion of the each panel at  $1.0 \mu\text{m}$  shows the particle size cut-off diameter below which fluorescent particles were not considered as FBAP due to potential interference with non-biological aerosol particles. (a) averaged over entire campaign, (b) Jun, (c) Jul, and (d) Aug. Please refer to supplementary Figs. for corresponding TAP plots.

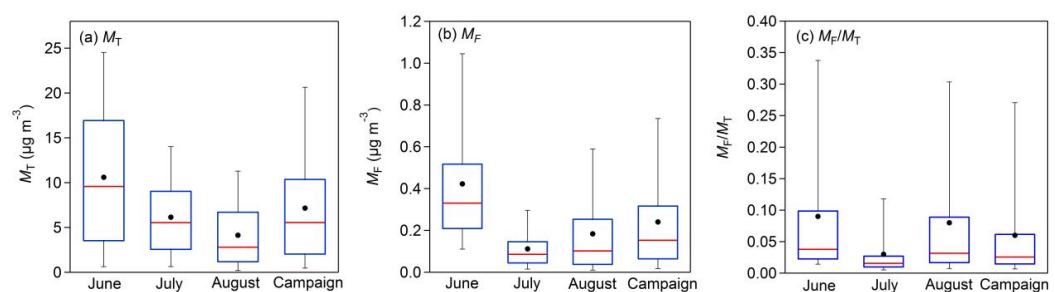


Figure 5: Same as Fig. 3 but for integrated ( $\sim 1 - 20 \mu\text{m}$ ) FBAP ( $M_F$ ) and TAP ( $M_T$ ) mass concentrations derived from number measurements by assuming unit density and shape factor.

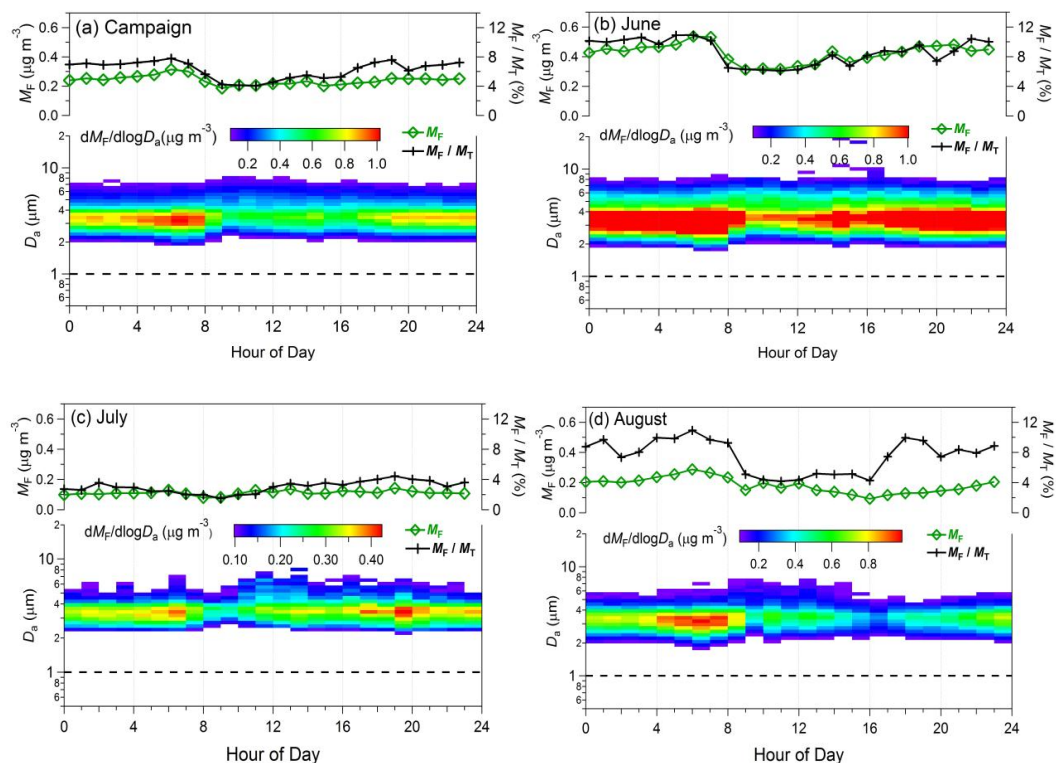


Figure 6: Same as Fig. 4 but representing the FBAP ( $M_F$ ) mass concentrations.

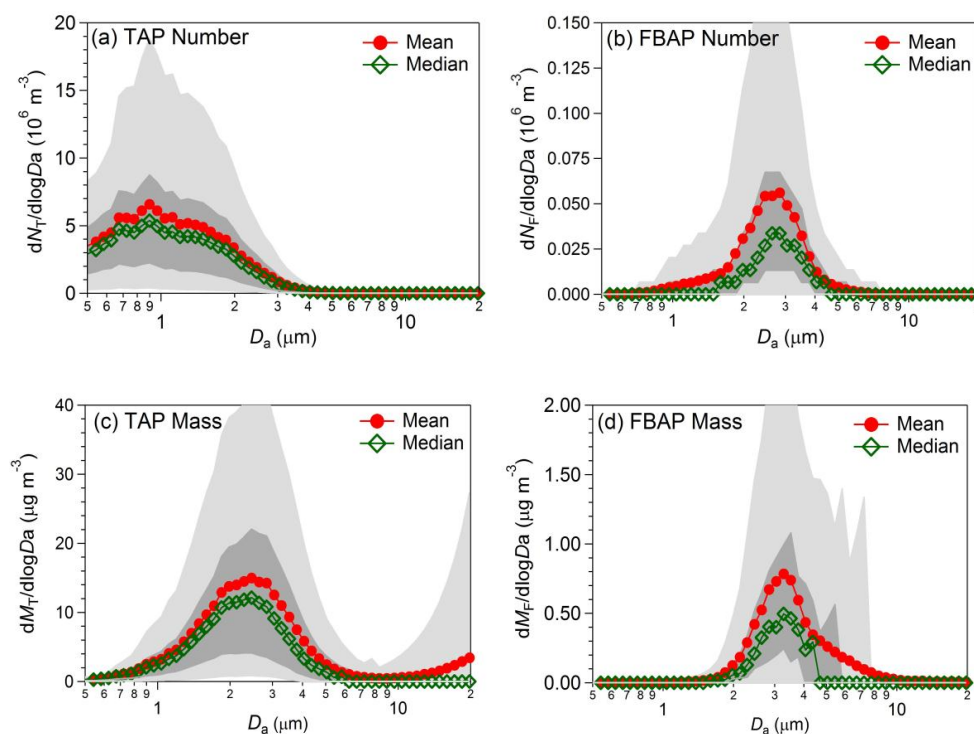


Figure 7: Particle number size and unit-normalized number size and mass size distributions averaged over the entire measurement campaign carried out at Munnar. Lower and upper parts of dark and light shaded area represents the 5<sup>th</sup>, 25<sup>th</sup>, 75<sup>th</sup>, and 95<sup>th</sup> percentile respectively. (a) TAP number ( $dN_T/d\log D_a$ ), (b) FBAP number ( $dN_F/d\log D_a$ ), (c) total mass ( $dM_T/d\log D_a$ ), and (d) FBAP mass ( $dM_F/d\log D_a$ ).

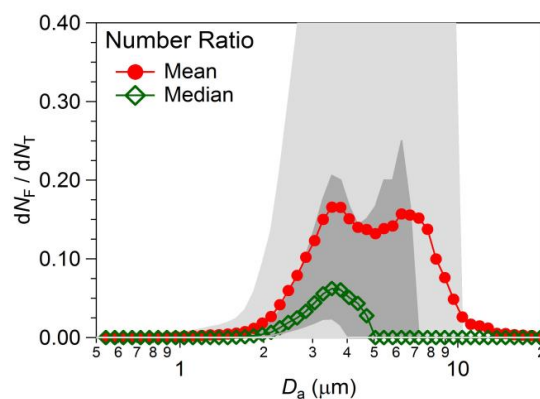


Figure 8: Size distribution of FBAP to TAP ratio averaged over the entire measurement period carried out at Munnar ( $dN_F/d\log D_a = dM_F/d\log D_a$ ). Lower and upper parts of dark and light shaded area represents the 5<sup>th</sup>, 25<sup>th</sup>, 75<sup>th</sup>, and 95<sup>th</sup> percentile respectively.

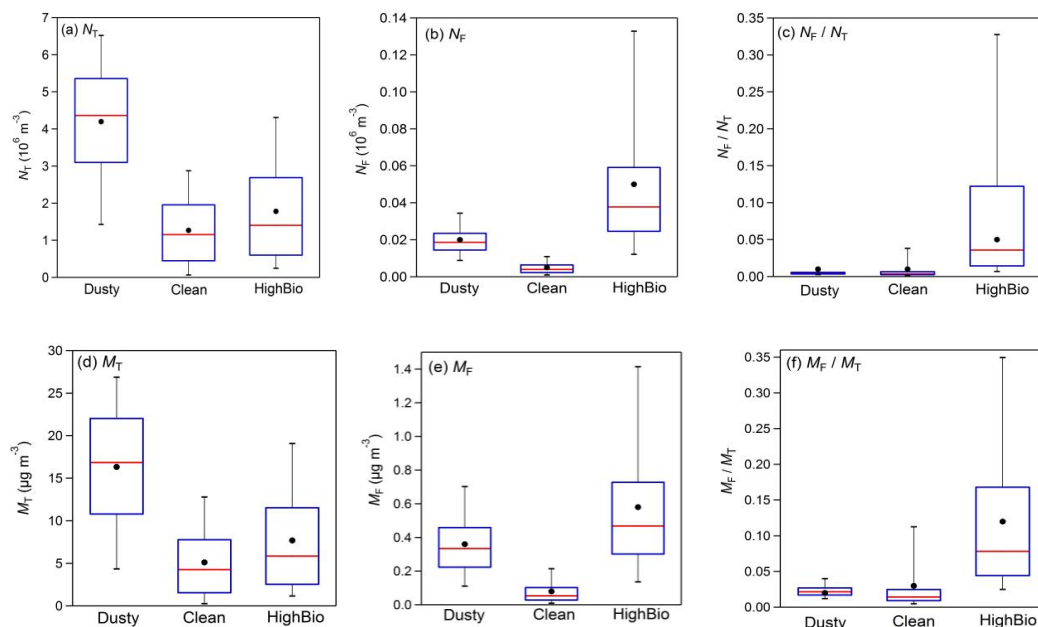


Figure 9: Statistical distribution of integrated ( $\sim 1 - 20 \mu\text{m}$ ) FBAP and TAP number and mass contribution of  $N_F$  to  $N_T$ , and  $M_F$  to  $M_T$  averaged over each distinct focus periods (dusty, clean, and high bio; please refer to the text for definitions related to each focus period) measurements carried out at Munnar as box whisker plots: (a) TAP number concentration ( $N_T$ ), (b) FBAP number concentration ( $N_F$ ), (c) contribution of FBAP number concentration to TAP number concentration ( $N_F/N_T$ ), (d) TAP mass concentration ( $M_T$ ), (e) FBAP mass concentration ( $M_F$ ), and (f) contribution of FBAP mass concentration to TAP mass concentration ( $M_F/M_T$ ).

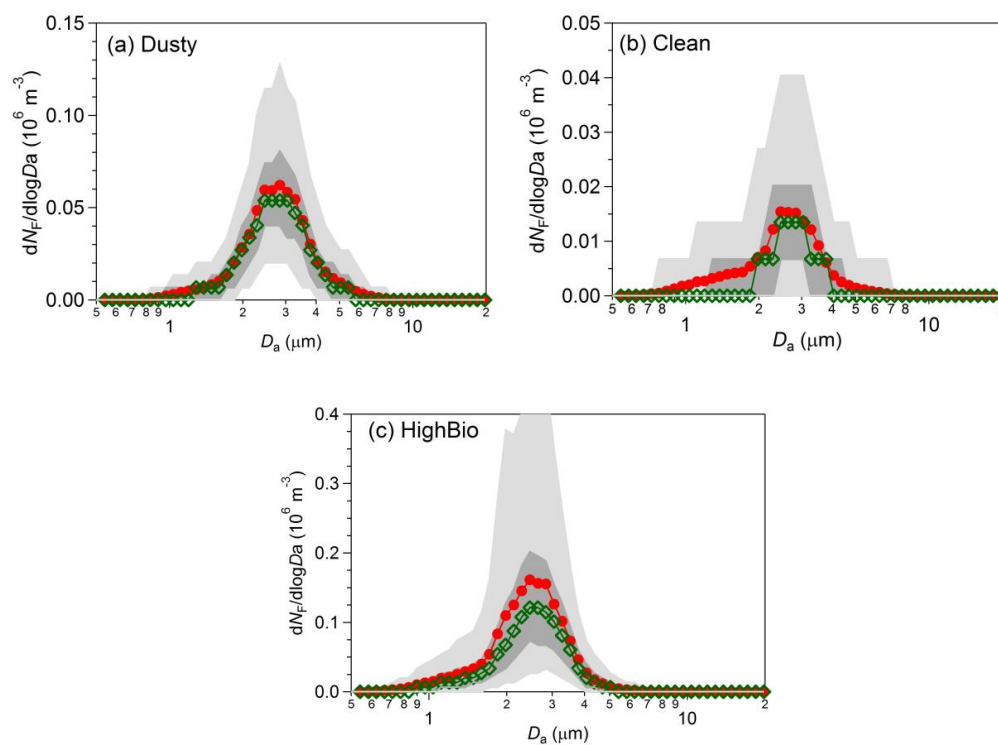


Figure 10: FBAP number size distributions ( $dN_F/d\log D_a$ ) averaged over each distinct focus periods during the measurement campaign carried out at Munnar. Lower and upper parts of dark and light shaded area represents the 5<sup>th</sup>, 25<sup>th</sup>, 75<sup>th</sup>, and 95<sup>th</sup> percentile respectively. (a) dusty period, (b) clean period, and (c) high bio period.



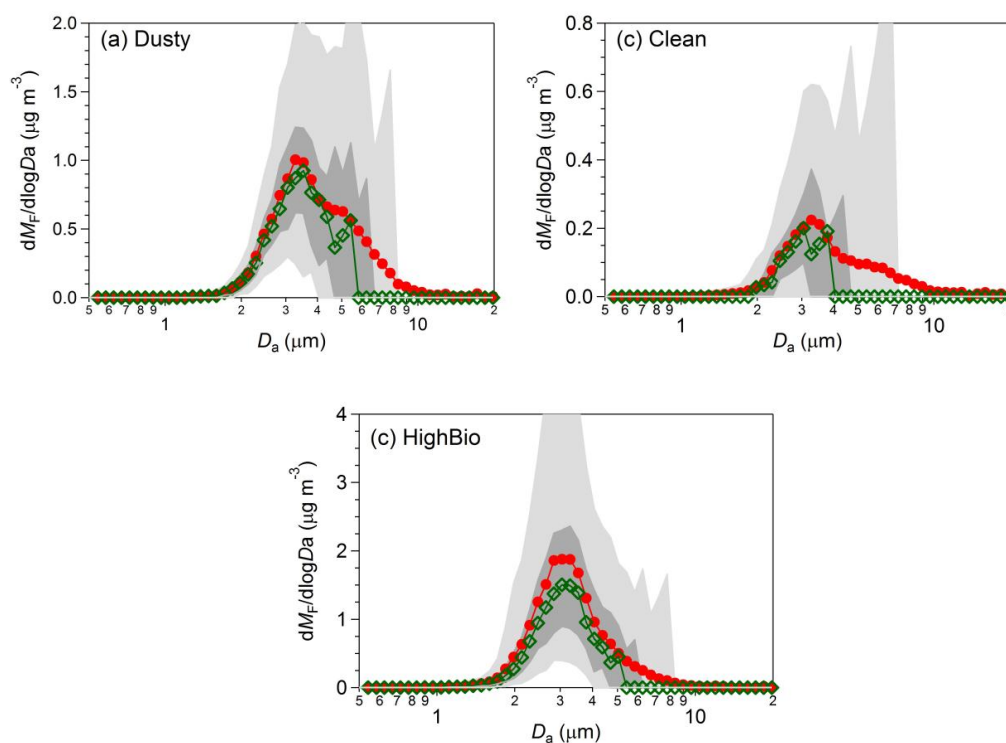


Figure 11: Same as Fig. 10 but representing FBAP mass size distribution ( $dM_F/d\log D_a$ ).

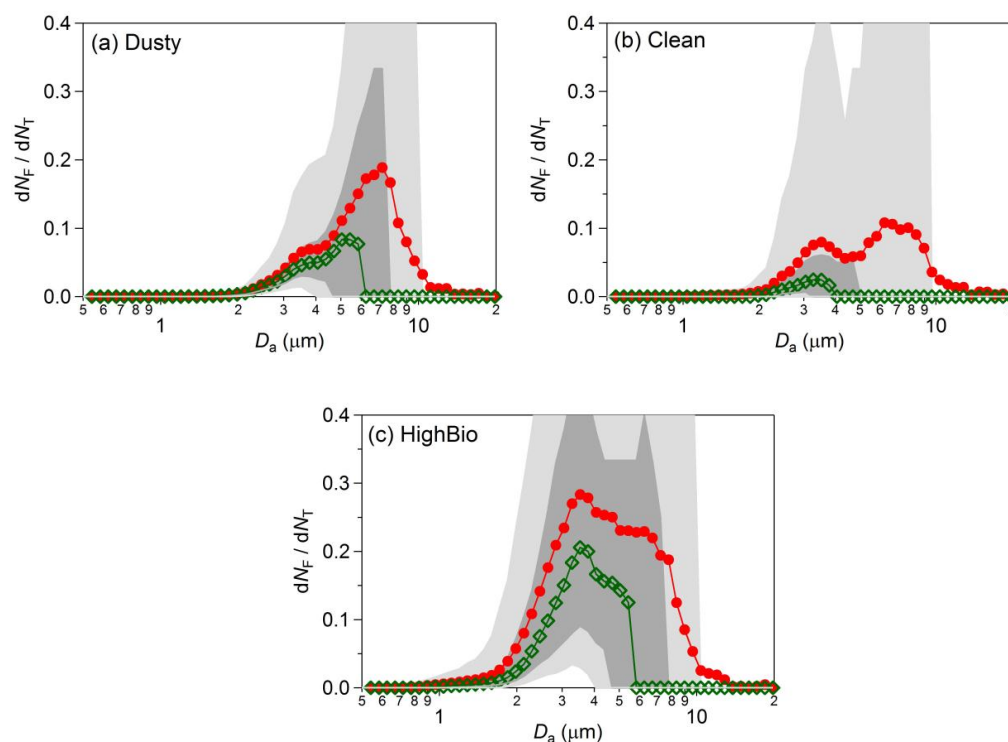


Figure 12: Size distribution of FBAP to TAP ratio averaged over the each distinct focus periods during the measurements carried out at Munnar ( $dN_F/d\log D_a = dM_F/d\log D_a$ ). Lower and upper parts of dark and light shaded area represents the 5<sup>th</sup>, 25<sup>th</sup>, 75<sup>th</sup>, and 95<sup>th</sup> percentile respectively: (a) dusty, (b) clean, and (c) high bio.

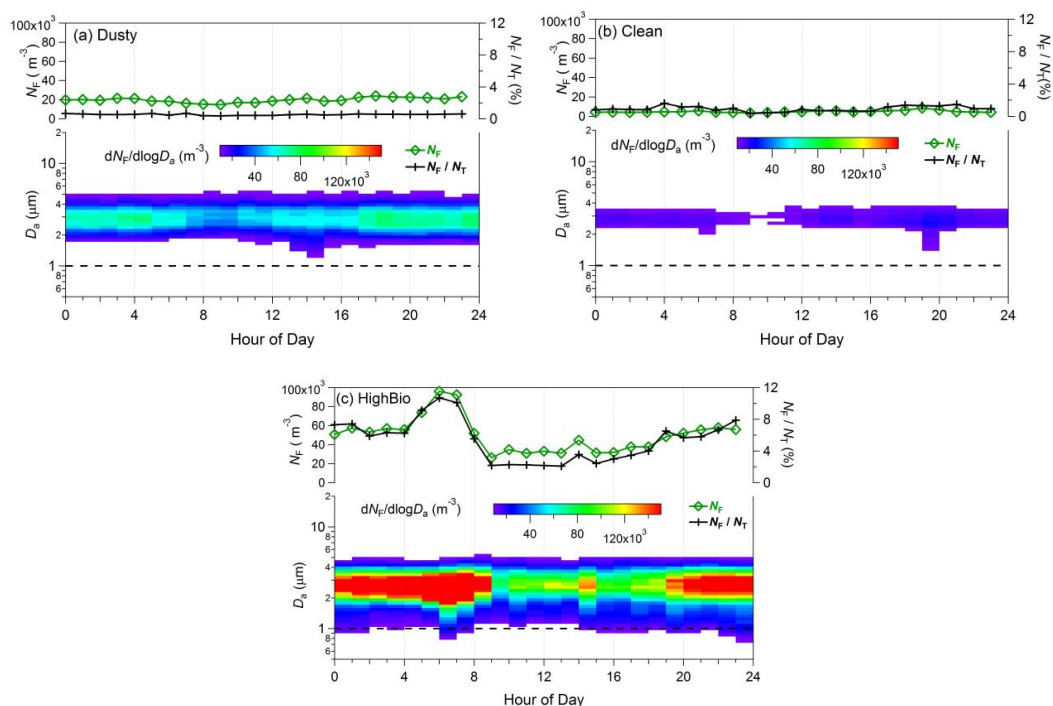


Figure 13: Diurnal cycles of FBAP number concentrations ( $N_F$ ) and size distributions averaged over each distinct focus period identified during measurements carried out at Munnar (hourly median values plotted against the local time of the day). Upper portion of each panel shows integrated FBAP number concentration ( $\sim 1 - 20 \mu\text{m}$ ;  $N_F$ ) on the left axis (green color) and FBAP fraction of TAP number ( $N_F/N_T$ ) on the right axis (black color). Lower portion of each panel FBAP number size distribution (3-D plot) plotted against hour of the day on x-axis, aerodynamic diameter on y-axis and color is scaled for  $dN_F/d\log D_a$  indicates the concentration. Dashed black lines in lower portion of the each panel at  $1.0 \mu\text{m}$  shows the particle size cut-off diameter below which fluorescent particles were not considered as FBAP due to potential interference with non-biological aerosol particles. (a) dusty (b) clean, and (c) high bio. Please refer to supplementary Figs. for corresponding TAP plots.

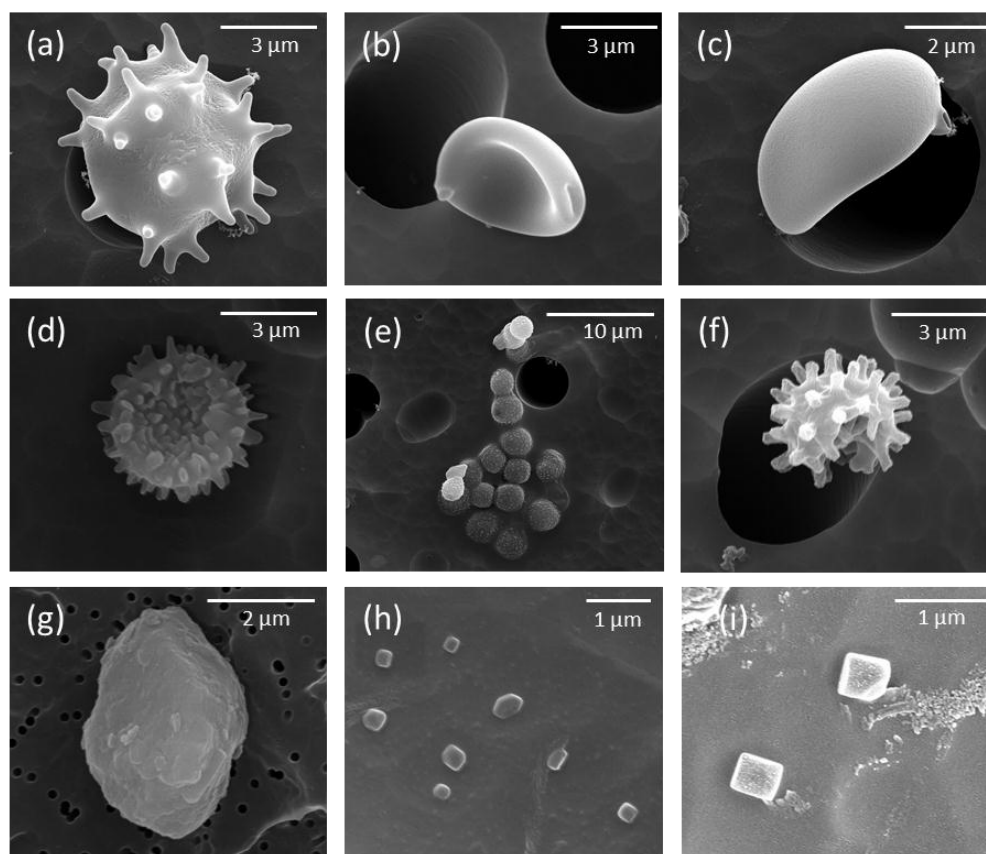


Figure 14: Scanning electron microscope images of the exemplary aerosol particles (FBAP and TAP) observed during the campaign at Munnar. The scale bar is shown at the top right corner of each image.

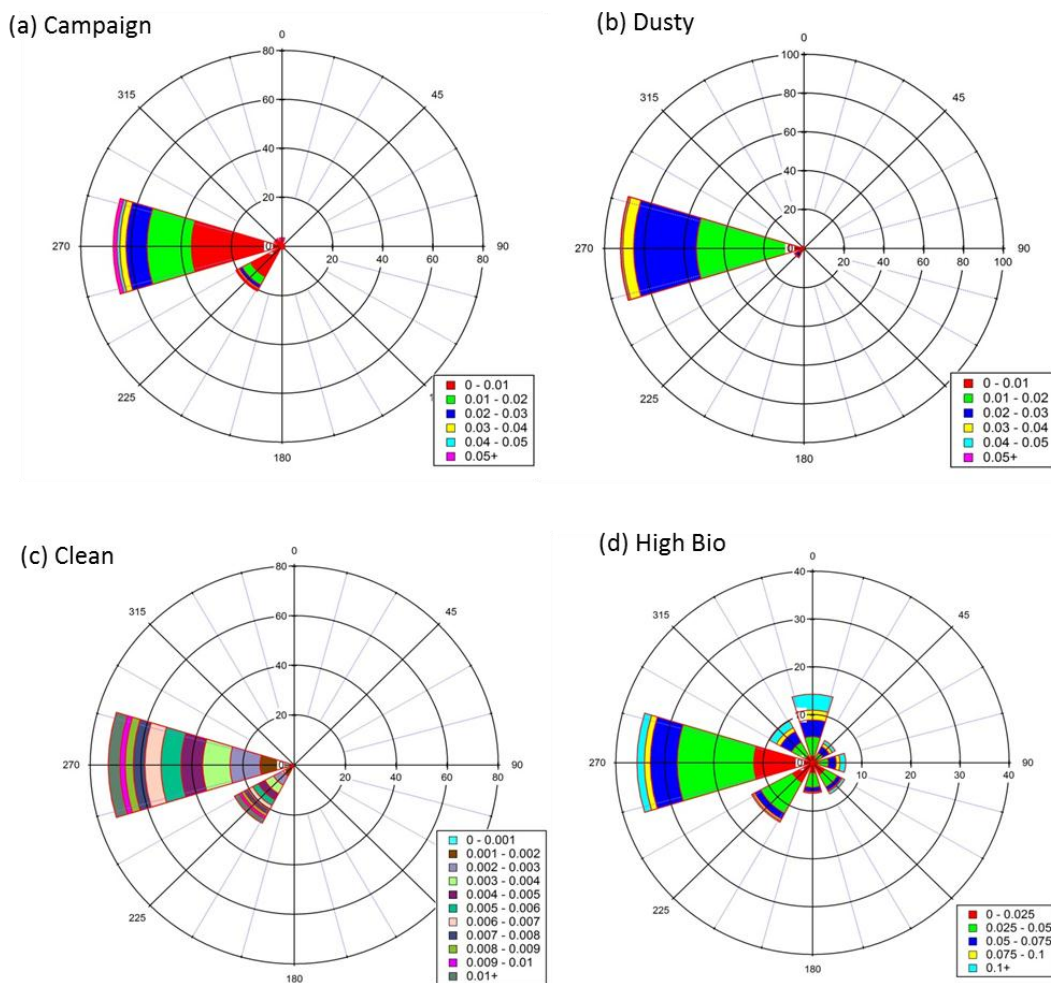


Figure 15: Wind rose diagram scaled over FBAP number concentration ( $N_F$ ). These diagrams in a way are similar to the traditional wind rose diagram except representing the  $N_F$  in this case instead of wind speed. These diagram can be nominally interpreted as followed: For example (a) shows that ~52% of frequency of occurrence of  $N_F$  concentration in the range of 0 – 0.001  $\text{cm}^{-3}$  was associated with Westerly/Southwesterly winds and on the contrary (d) indicates that out ~18% of frequency of occurrence of high concentration ( $N_F > 0.1 \text{ cm}^{-3}$ ) ~16% was associated with Northerly/Northwesterly winds. (a) entire campaign, (b) dusty period, (c) clean period, and (d) high bio period.

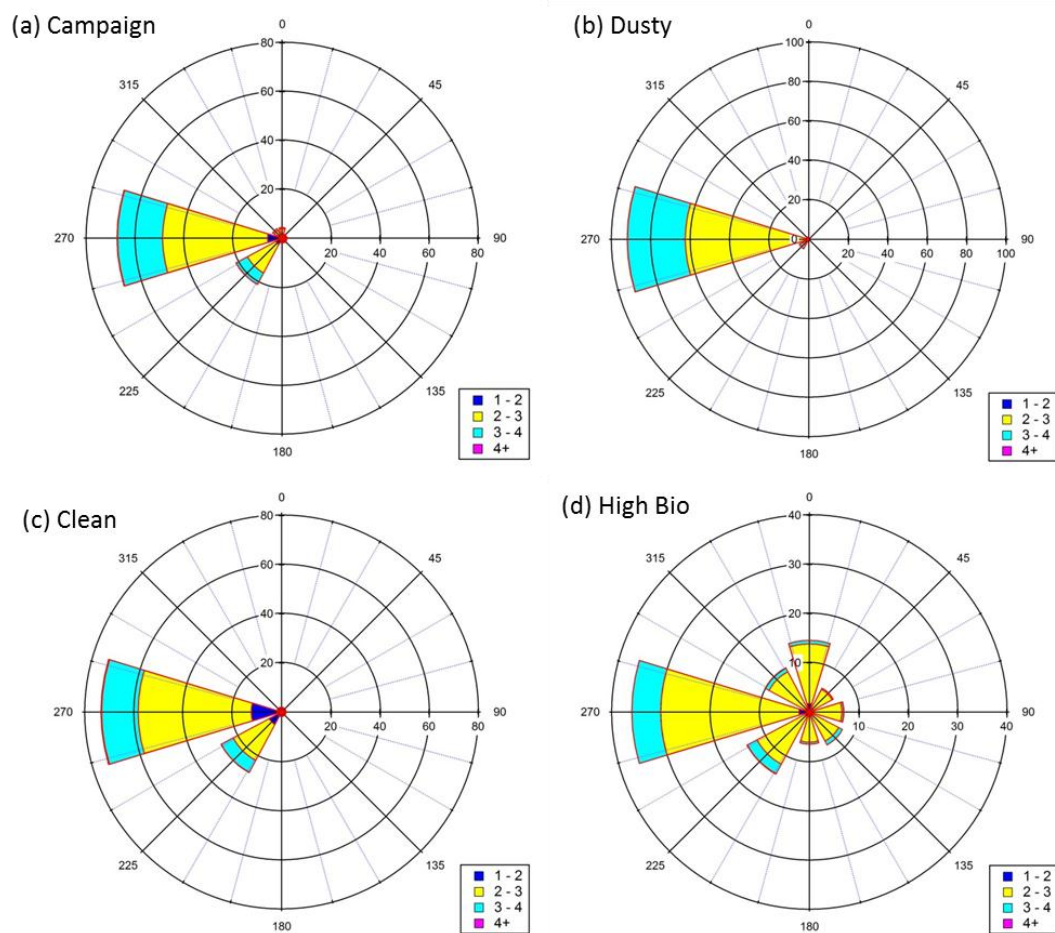


Figure 16: Same as Fig. 18 but scaled by geometric mean diameter ( $D_g$ ) of  $dN_F/d\log D_a$ . (a) entire campaign, (b) dusty period, (c) clean period, and (d) high bio period.



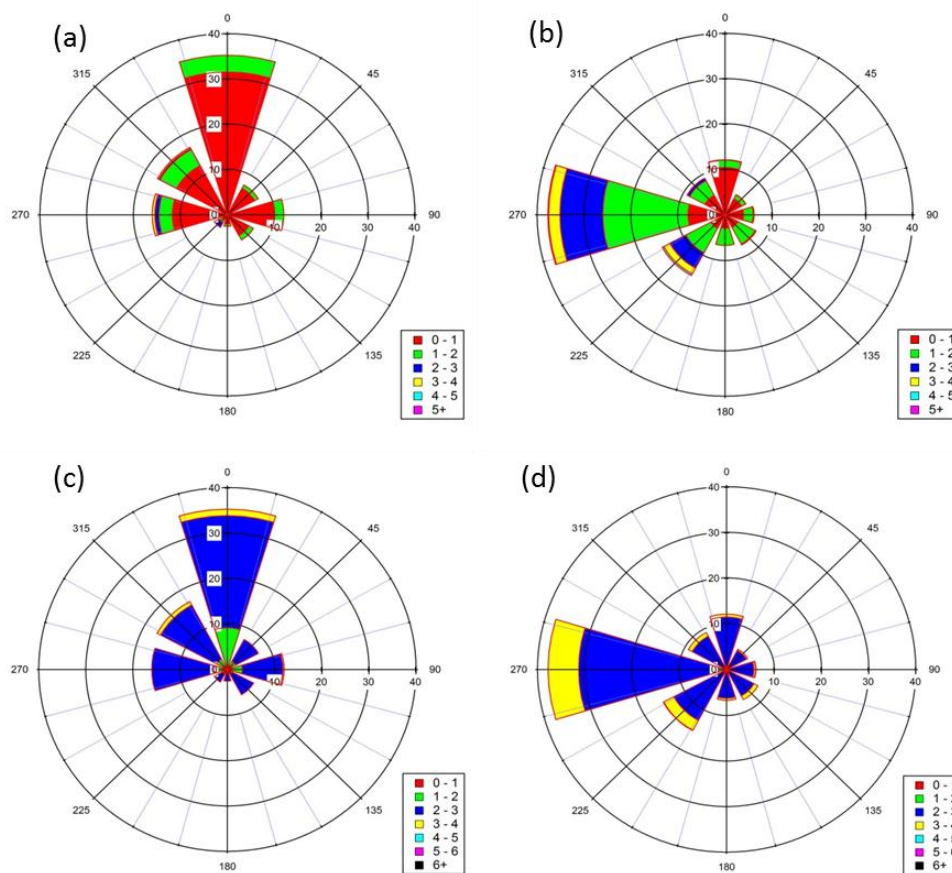


Figure 17: Wind rose diagram scaled by wind speed and geometric mean diameter ( $D_g$ ) of  $dN_F/d\log D_a$ . The figures have been separated for FBAP number concentration ( $N_F$ ) range,  $N_F > 0.1 \text{ cm}^{-3}$  and  $N_F < 0.1 \text{ cm}^{-3}$  observed during high bio period. For example: when,  $N_F > 0.1 \text{ cm}^{-3}$  ~60% of the time wind was observed to be in the range of  $0 - 1 \text{ m s}^{-1}$  (a) and ~94% of the time the geometric mean diameter ( $D_g$ ) of  $dN_F/d\log D_a$  was in the range of  $2 - 3 \mu\text{m}$  (c). On the other hand for  $N_F < 0.1 \text{ cm}^{-3}$  ~60% of the time wind was greater than  $1 \text{ m s}^{-1}$  (b), and ~80% of the time geometric mean diameter ( $D_g$ ) of  $dN_F/d\log D_a$  was in the range of  $2 - 3 \mu\text{m}$  (d).

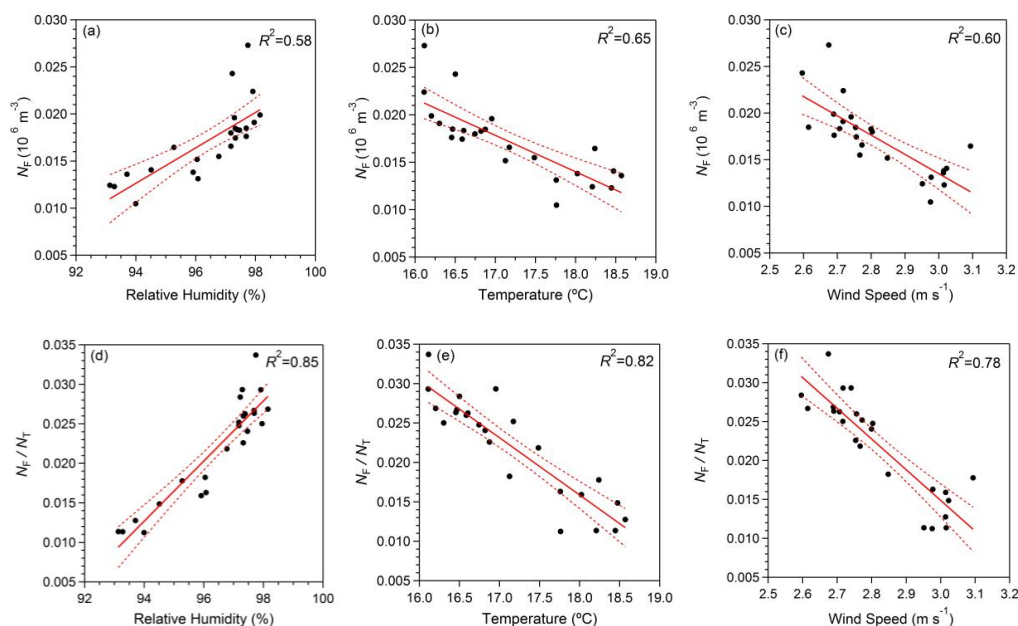


Figure 18: Correlation between aerosol particle number concentrations ( $N_F$ ,  $N_T$ , and  $N_F/N_T$ ) and meteorological parameters (relative humidity, temperature, and wind speed). Red line indicates the best fit to the scattered points and dashed black line indicates the 95% confidence level obtained for the best fit.